Forschungszentrum Karlsruhe
Technik und Umwelt

Wissenschaftliche Berichte
FZKA 5679

Comparison of the Quench Experiments CORA-12, CORA-13, CORA-17

S. Hagen, P. Hofmann, V. Noack, L. Sepold,
G. Schanz, G. Schumacher

Hauptabteilung Ingenieurtechnik
Institut für Materialforschung
Institut für Neutronenphysik und Reaktortechnik
Projekt Nukleare Sicherheitsforschung

August 1996

Forschungszentrum Karlsruhe

Technik und Umwelt

Wissenschaftliche Berichte

FZKA 5679

Comparison of the Quench experiments CORA-12, CORA-13, CORA-17

S. Hagen, P. Hofmann, V. Noack, L. Sepold,
G. Schanz, G. Schumacher

Hauptabteilung Ingenieurtechnik
Institut für Materialforschung
Institut für Neutronenphysik und Reaktortechnik
Projekt Nukleare Sicherheitsforschung

Forschungszentrum Karlsruhe GmbH, Karlsruhe
1996

Forschungszentrum Karlsruhe GmbH
Postfach 3640, 76021 Karlsruhe

ISSN 0947-8620

ABSTRACT

The CORA quench experiments 12, 13 (PWR) and 17 (BWR) are in agreement with the inpile tests LOFT LP-FP-2 and PBF SFD-ST and the TMI accident: Flooding of hot Zircaloy clad fuel rods does not result in an immediate cooldown of the bundle, but produces a remarkable temporary temperature increase connected to a strong peak in hydrogen production.

For the preparation of new quench bundle tests, necessary for the understanding of the mechanisms governing the quench process and support for validation of future quench models in SFD codes the three tests are compared to each other and to the relevant non-quench tests CORA-29 (PWR) and CORA-16 (BWR).

The PWR tests CORA-12 and CORA-13 are of the same geometrical arrangement and test conduct. An exception is the shorter time between power shutdown and quench initiation for CORA 13, resulting in a higher temperature of the bundle at start of quenching.

The BWR test CORA-17 used B_4C absorber and Zircaloy channel box walls, but was in respect to the delay time between power shutdown and start of quenching similar to test CORA-12.

All three tests showed during the quench phase the temporary temperature increase correlated to a hydrogen peak. In test CORA-12 with a delay of 300 s between power shutdown and start of quenching, resulting in a cooldown of more than 100 K, a delay of about 50 s was registered between start of quenching and the initiation of the increase of temperature and hydrogen production.

The water level at this time had already reached the elevation of about 200 mm. In test CORA-13 with a start of quenching 30 s before power shutdown, temperature and hydrogen production increase started immediately after start of quenching.

Immediately after quenching BWR test bundle CORA-17 experiences a modest increase for 20 s and changed then in a steep increase resulting in the highest temperature and hydrogen peaks of the three tests. CORA-17 also showed a temperature increase in the lower part of the bundle, in contrast to CORA-12 and CORA-13 with temperature increase only in the upper half of the bundle. We interpret this earlier starting and stronger reaction due to the influence of the boron carbide, the absorber material of the BWR test.

B_4C has a exothermic reaction energy 4 to 5 times larger than Zry and produces about 6 times more hydrogen. Probably the hot remained columns of B_4C (seen in the non-quench test CORA-16) react early in the quench process with the

increased upcoming steam. The bundle temperature, raised by this reaction increases the reaction rate of the remained metallic Zry (exponential dependence). Due to the larger amount of Zry in the BWR bundle (channel box walls) and the smaller steam input during the heatup phase (2 g/s instead of 6 g/s) more metallic Zry can have survived oxidation during the heatup phase.

The different behavior of the three tests provides a good basic for the validation of further quench models.

Kurzfassung: Vergleich der Quenchexperimente CORA-12, 13,17

Die Quenchexperimente CORA-12, CORA-13 und CORA-17 zeigten ebenso wie die Inpile-Experimente LOFT LP-FP-2 und PBF SFD-ST in Übereinstimmung mit dem TMI 2-Störfall beim Fluten des überhitzten Bündels vor dem endgültigen Abkühlen einen starken Temperaturanstieg, der mit einer heftigen Wasserstoffentwickung verbunden war.

Als Vorbereitung für neue Quench-Bündelversuche und für die Überprüfung von Quench-Modellen in SFD-Rechenprogrammen wurden die drei Experimente miteinander und mit den entsprechenden Nicht-Quench-Experimenten CORA-29 (DWR) und CORA-16 (SWR) verglichen.

Der Unterschied zwischen den Druckwasserreaktor-Experimenten CORA-12 und CORA-13 lag in der kürzeren Zeit zwischen Ende der elektrischen Energiezufuhr und Quenchbeginn für CORA-13, was eine höhere Bündeltemperatur beim Quenchbeginn zur Folge hatte. Das SWR-Experiment CORA-17 mit B_4C-Absorber und zusätzlich simulierten Zircaloy-Kanalwänden war in Bezug auf die Verzögerungszeit zwischen Ende der elektrischen Energiezufuhr und Quenchbeginn dem Versuch CORA-12 ähnlich.

Vor der endgültigen Abkühlung zeigten alle drei Versuche während der Flutphase einen zwischenzeitlichen Temperaturanstieg, der mit einem Peak in der Wasserstofferzeugung verbunden war. Im Versuch CORA-12 lag eine Verzögerung von 300 s zwischen dem Abschalten der Leistung und Flutbeginn mit einer Abkühlung von gut 100°C vor. Dies hatte eine Verzögerung von ca. 50 s zwischen dem Flutbeginn und dem Anstieg von Temperatur und Wasserstoffproduktion zur Folge. Der Wasserspiegel hatte in dieser Zeit schon eine Bündelhöhe von ca. 200 mm erreicht. Im Versuch CORA-13, mit einem Flutbeginn von 30 s vor Leistungsabschaltung, stiegen Temperatur und Wasserstofferzeugung unmittelbar nach dem Flutbeginn an.

Der Siedewasserreaktor-Versuch CORA-17 zeigte nach dem Flutbeginn für 20 s einen leichten Anstieg und wechselte dann in einen steilen Anstieg für Temperatur und Wasserstoff über. Von den drei Quenchexperimenten hatte CORA-17 den stärksten Anstieg in der Temperatur und in der Wasserstofferzeugung.

Im Siedewasserreaktor-Versuch war im Gegensatz zu den beiden DWR-Versuchen auch im unteren Bereich des Bündels einen Temperaturanstieg zu erkennen. Wir führen den beschriebenen Unterschied auf den Einfluß des Borkarbids, dem Absorbermaterial des Siedewasserreaktors, zurück.

Der Energiegewinn bei der Borkarbid/Wasserdampf-Reaktion ist 4 bis 5 mal größer als bei der Zry/Wasserdampf-Reaktion und erzeugt auch ca. 6 mal mehr Wasserstoff. Wir nehmen an, daß die heißen gesinterten Restsäulen, sichtbar im Nicht-Quenchtest CORA-16, beim einsetzenden Quenchvorgang mit dem stark zunehmenden Dampfstrom reagieren.

Die durch diese Reaktion erhöhte Bündeltemperatur bewirkt eine erhöhte Reaktionsrate des verbleibenden metallischen Zry (exponentielle Abhängigkeit von der Temperatur). Die größere Zry-Menge im SWR-Bündel (zusätzlich BE-Kanalwände) und die geringere Dampfeinspeisung während der Aufheizphase, d.h. 2 g/s anstatt 6 g/s kann eine größere Restmenge metallischen Zircaloys beim Quenchbeginn ermöglichen. Das unterschiedliche Verhalten der drei Versuche bietet eine gute Möglichkeit für die Überprüfung zukünftiger Quenchmodelle in Rechen-Programmen.

Contents

1. Introduction

Three of the nineteen CORA-tests were completed by quenching. As the most important results CORA-12, CORA-13 and CORA-17 showed a preliminary temperature increase in coincidence with a peak in the hydrogen production before the final cooldown. This is in agreement with the results of the PBF SFD-ST, and LOFT LP-FP2 quench experiments as well as the TMI accident.

These phenomena can be explained by the exothermic zirconium-steam reaction. Without knowing the mechanisms in detail, we have to assume that the ZrO_2 layer of the Zry cladding looses its protective character to a large extent during the quench process. The smooth protective ZrO_2 layer, growing during heatup, results in an oxidation reaction reciprocal to the layer thickness. Cracks or spallations caused by the quench process would allow the steam to access the hot metallic Zry. The Zr/steam reaction, growing exponentially with temperature would result in the measured temperature escalation, parallel to the corresponding hydrogen production.

In this report, we compare the temperature and hydrogen production behavior of the three tests to the respective non-quench tests and among each other. These comparisons prove, that the temperature and hydrogen peak are connected to the quench process. But it also shows a higher temperature and hydrogen increase in BWR test CORA-17 than in PWR tests CORA-12 and CORA-13. In CORA-17 to the start of the quench process, the increase of temperature and hydrogen is found earlier.

We assume that this additional temperature increase and production of hydrogen is caused by the remnants of the B_4C absorber which is present only in the BWR test.

2. Test description

The CORA out-of-pile facility was designed to investigate the behaviour of LWR fuel elements under severe fuel damage accident conditions. In the experiments the decay heat was simulated by electrical heating. Great emphasis was put on the fact that the test bundles contain all materials used in light-water reactor fuel elements to investigate the different material interactions. Pellets, claddings, grid spacers, absorber rods and the pertinent guide tubes were typical to those of commercial LWRs with respect to their compositions and radial dimensions.

Figure 1 gives a simplified flow diagram of the CORA facility and Figure 2 the arrangement of the facility. The central part of the facility was the fuel rod

bundle. The bundle was enclosed in a Zry-shroud with ZrO_2 fibre insulation. A high- temperature radiation shield surrounded the bundle, leaving an annular space for moving up the quench cylinder. The bundle was connected to the power supply system at the upper and lower end.

Below the bundle was the quench unit with a water-filled quench cylinder, which could be raised with a controlled speed. The cylinder was guided by three rods, which also connected the electric power to the bundle lower end. At the beginning of the test the water level was 220 mm below the "zero elevation" of the bundle. The "zero elevation" corresponded to the lower end of the pellets in the heated rods.

The upper end of the fixed bundle was at the bundle head plate. The plate was connected by a funnel-shapped tube to the surge condenser. The surge condenser was double-walled, leaving access to the bundle end fittings above the bundle head funnel.

The steam was produced in the steam generator, superheated and led to the lower end of the bundle, entering at "zero elevation". The steam not consumed within the bundle was condensed into two parallel condensers and the hydrogen produced was given to the off-gas system after dilution to low H_2 concentration by air.

The arrangements of the PWR and BWR bundles can be seen from Figure 2. We used heated and unheated fuel rod simulators. Both types were sheathed with standard Zircaloy-4 cladding (10,75 mm outer diameter). The central part of the heated fuel rod consisted of a 6 mm tungsten rod surrounded by UO_2 annular pellets. The tungsten heater had an effective length of 1024 mm. At the top and the bottom the tungsten heater is screwed into Mo-electrodes of 300 mm length which fitted directly into the Zry cladding. The molybdenum electrodes were connected to copper electrodes and both were electrically insulated from the Zircaloy cladding by a flame-sprayed ZrO_2 layer. The unheated fuel rod contained solid UO_2 pellets.

The standard PWR bundle consisted of 16 heated, 7 unheated and two absorber rods. They were composed of original components. The (Ag80, In15, Cd5) absorber material was sheathed in stainless steel and this rod was surrounded by a Zry guide tube. Three spacers were used in the bundle to maintain the geometry. The material of the middle spacer was Inconel 718 and the upper and lower were made of Zry-4.

The BWR bundle simulated the arrangement of the absorber placed between the bundles which are surrounded by a channel box. The original B_4C powder/stainless steel rods inside the stainless steel blade were separated from the fuel rod simulators by the Zry channel box walls.

The bundle was surrounded by a Zry-4 shroud of 1.2 mm thickness. The steam entered the bundle at 180° and at the 0 mm elevation. To minimize the heat losses, the shroud was surrounded by an insulating layer of ZrO_2 fibre of 19 mm (0.75 inch) thickness. Since the ZrO_2 fibre layer has a low heat conductivity and heat capacity, the shroud temperatures could follow the bundle temperature closely. Since the Zry shroud participates in the interaction with steam, the resulting oxidation energy contributes substantially to the bundle heatup.

To keep the heat losses as low as possible, the bundle was additionally surrounded by a high-temperature shield. This shield consisted mainly of ceramic fibre plates (inner plates ZrO_2; outer plates Al_2O_3).

The power input was controlled by measuring the currents of the single rods and settings of the common voltage necessary to obtain the desired power history. The electric heating by direct current avoided the generaton of eddy currents in the structures of the facility..

3. Test conduct

Generally the tests were performed following the same procedure for each test. It can be divided into three phases (Figure 3-7).

1. gas preheat phase 0 - 3000 s
2. transient phase 3000 - 4900 s (about)
3. quench or cooling phase.

In the gas preheat phase there wasa flow of 8 g/s preheated argon and a low constant electric power input of about 0.65 kW. During this period the temperature in the insulation reached a level which was high enough to avoid steam condensation. To keep the videoscope windows clear, a total flow of 1 g/s argon was directed to the front of the windows of the videoscopes. The pressure in the system was controlled to 0.22 MPa (absolute).

During the transient phase the temperature increase of initially 1 K/s was achieved by rising the electric power input from 6 to 27 kW in the PWR tests and

from 6 to 26 kW in the BWR tests. At 3300 s an additional steam flow of 6 g/s for the PWR tests and of 2 g/s for the BWR tests was added to the test section.

The electric power input was terminated at about 4900 s. For comparison, tests CORA-29 and CORA-16 then started the slow cooling phase. In test CORA-13 the flooding phase was initiated 30 s before the initiation of power shutdown (Fig. 8). In consequence, the quench process started at the maximum temperature. In tests CORA-12 and CORA-17 the initiation of quenching was delayed by about 150 s after the shutdown of power (Figure 8), which allowed a certain cooldown of the bundle.

The flooding of the bundle was performed by hydraulically rising the water-filled quench cylinder. Due to experimental reasons the rise of the cylinder had to be performed in a stepwise manner to reach the mean increase of 1 cm/s. A period of faster increase is always followed by a resting phase. The time history for the elevation of the upper edge of the quench cylinder and the water in the quench cylinder is given in Figures 9 to 11. The water level in the quench cylinder was determined by measuring the pressure difference of the water column. The decrease of the water level during the resting phse of quench cylinder gives the evaporation of the water from the quench cylinder. The strong fluctuation in the signal in the upper part of the bundle was caused by the strong agitation in quenching the bundle of very high temperature.

From time history of the water level in the quench cylinder the evaporation rate during the quench process was determined, taking into account the additionally added water to the quench cylinder. The results are given in Figure 12 for CORA-13 and CORA-17.

4. Comparison of results

4.1 Temperature escalation outside the bundle

In the quench tests the flooding process is accomplished by moving up the water-filled quench cylinder. Therefore all thermocouples must be introduced into the bundle from the top. In consequence, more thermocouples were destroyed within the bundle towards the end of the test. The innermost positions outside the bundle at which the thermocouples completely survived, were located at the inner wall of the high-temperature shield. There the temperature was measured at different elevations. In Figures 13 to 15 for the three tests CORA-12, CORA-13 and CORA-17 the temperatures at the inner wall were compared to those measured in the relevant non-quench test: CORA- 29 for the PWR and CORA-16

for the BWR bundle. The temperatures measured on the inside of the high-temperature shield were delayed to the temperatures inside the bundle, but they represent the temperature behaviour of the bundle very well, having the advantage of showing results for the whole test time at all elevations.

In Figure 13 the comparison of CORA-12 to CORA-29 shows up to the quench initiation at all elevations the same behaviour for the temperatures measured at different elevations: a temperature increase similar as in the bundle during the heating phase, which changes into a temperature decrease after shutdown of the electric power. The general lower temperatures in test CORA-12 was caused by the lower temperature of the incoming argon during the gas preheating phase. The influence of quenching in test CORA-12 resulted in a sharp temperature decrease up to 390 mm and a temporary increase above 590 mm elevations.

In Figure 14, test CORA-13, compared to CORA-29 confirms the results found for CORA-12. Due to the same temperatures of the incoming argon during the gas preheat phase the general temperature level was the same for CORA-13 and CORA-29. In CORA-13 the quench process was started 30 s before the initiation of the power shutdown. As a result, the temperature increase took place immediately after the heating phase. The temperature increase was larger than in test CORA-12.

For BWR test CORA-17 the influence of quenching was much more pronounced. The lower temperature level before quenching was due to the temperatures of argon during the gas preheat phase for CORA-17 and CORA-16. But a much higher temperature increase due to quenching was reached for the BWR bundle. Also a slight temperature increase started already at the lowest measured elevation. This temperature increase already at low elevations is also seen in the measurements of the temperature on the outside of the bundle insulation as shown in Figure 16.

4.2 Temperature escalation inside the bundle compared to the hydrogen production.

The temperature behaviour of the bundle in comparison to the hydrogen production is presented in Figures 17 to 19. For each of the three tests temperatures are given at three elevations in the upper part of the bundle between 750 mm and 1350 mm. The relative time dependence of the hydrogen production was measured in the off-gas-system.

The temperature measurements in the bundle confirm the behaviour found on the inner wall of the high-temperature shield: All tests resulted in preliminary temperature increase due to the quench process. The delay between power shutdown and quench initiation in CORA-12 resulted also here in a temperature decrease earlier to the quench-caused temperature peak. Due to the higher starting temperature the temperature increase was larger for CORA-13 as compared to CORA-12. But the most pronounced temperature peaks were found for BWR test CORA-17 though also CORA-17 had a cooldown period between electric energy shutdown and quench initiation. The hydrogen production in all three tests is unambiguously correlated to the temperature of the respective bundle. Again the hydrogen production was higher in CORA-13 than in CORA-12 and significantly more hydrogen was produced in CORA-17.

Figures 20 to 22 give in addition the temperature peaks measured in the three tests.

4.3 Time delay of the quench reaction

The build-up of the temperature and hydrogen peaks relative to the quench initiation in Figures 17 to 19 show a different delay behaviour for the three tests. For comparison with SFD code calculations the shape of temperature and hydrogen peaks relative to the quench initiation are given in Figures 23 to 25. Always the relative hydrogen production, the temperature peak and the water level in the quench cylinder are given. In all three tests the close correlation between temperature and hydrogen increase can be seen. In test CORA-13 the reaction rate (temperature, hydrogen production) increased practically together with the quench initiation (30 s before electric power shutdown). The cooldown of bundle CORA-12, due to the delay between power shutdown and quench initiation, resulted in a delay between quench initiation and start of temperature and hydrogen increase.

For BWR test CORA-17 (Fig. 25) with a similar cooldown time as CORA-12 the delay after the quench initiation was shorter. In CORA-17 for 20 s a flat increase was found which then changed into a fast increase. As discussed later this different behaviour is assumed to have been caused by the remnant B_4C of the BWR absorber.

4.4 Explanation of the stronger reaction in the BWR test CORA-17

The comparisons discussed above show a significant higher temperature and hydrogen production increase during the quench process for the BWR test CORA-17. In CORA-17 the temperature increase is also found in the lower part of the bundle and there was a faster response after start of quenching compared to CORA-12, which is similar in respect to the delay time between power shutdown and quench initiation.

It is assumed, that the additional energy and hydrogen production was caused by steam reaction with the remnant B_4C absorber. The BWR test bundle contained eleven rods containing B_4C in an arrangement shown for test CORA-16 (Fig. 26). In the lower half of the bundle these control rods survived in the non-quench test in form of sintered columns as seen in Fig. 27. CORA-16 was performed exactly as CORA-12 without the quench process after the shutdown of the electric energy input. The appearance of the bundle at the end of CORA-16 is therefore representative for the conditions at the beginning of the quench process. This means B_4C is available for the reaction with steam. The equivalent cross sections for CORA-17 after the quench process show the dissappearance of the B_4C remnants.

In addition, B_4C oxidation in steam is more exothermic and produces more hydrogen per gramm material than Zircaloy.

Compared to

$$Zr + 2H_2O \rightarrow ZrO_2 + 2H_2$$

the B_4C oxidation in steam is more complicated /8/. Three reactions are possible.

$$B_4C + 8H_2O \rightarrow 2B_2O_3 + CO_2 + 8H_2 \quad \text{and/or}$$
$$B_4C + 7H_2O \rightarrow 2B_2O_3 + CO + 7H_2$$
$$B_4C + 6H_2O \rightarrow 2B_2O_3 + CH_4 + 4H_2$$

The B_2O_3 may react again with steam to form boric acids, depending on partial steam and hydrogen pressure.

$B_2O_3 + H_2O \rightarrow 2HBO_2$ (metaboric acid) and/or
$B_2O_3 + 3H2O \rightarrow 2H3BO3$ (orthoboric acid)
$3B_2O_3 + 3H_2O \rightarrow 2(HBO_2)_3$ (trimer of metaboric acid)

Due to thermodynamic considerations for B_4C only the first two and the fourth equation have a remarkable probability. The hydrogen production of 1 gram material is about 6 times larger for B_4C than for Zry. The maximum energy gain for 1 g B_4C may be maximal about 4 to 5 times larger than for 1 g Zry.

In 1 meter length the PWR bundle contains 3680 g Zry and the BWR bundle 5440 g Zry and 441 g B_4C. Due to the more effective reaction it is assumed that the B_4C contributes to the hydrogen production and heatup of the bundle. The initial reaction of the remnant B_4C in the lower part of the bundle increases the temperature so that the Zry reaction can take place at a higher level.

4.5 Summary and Conclusions

The comparison of the quench tests CORA-12, 13, 17 have clearly shown the following experimental results. Flooding of a hot Zircaloy-clad bundle does not decrease the temperature immediately but results in a preliminary increase before being quenched. The temperature peak is related to a peak in the hydrogen production. In the BWR bundle temperature and hydrogen increase is larger and starts also already earlier after quench initiation.

The phenomena described above - temperature- and hydrogen production increase during quenching for a zircaloy-clad bundle - are confirmed by the in-pile experiments performed by the Idaho National Engineering Laboratory. The LOFT LP-FP2 experiment (100 fuel rods 1.67 m long) as well as the Power Burst Facility SFD-ST test (32 fuel rods 0.91 m long) resulted in dramatic increase in temperature and hydrogen production during the reflood phase. In the LOFT test LP-FP2 during quenching peak temperatures increased from 2400 K to above 2800 K and 75% of the total hydrogen was produced during this phase.

In-pile as well as out-of-pile tests show a clear experimental evidence for the strong increase of the exothermic Zr/steam reaction during the quench process. This behaviour is intensified for the BWR bundle by the B_4C/steam reaction.

Without understanding the mechanisms in detail, we have to assume that the ZrO_2 layer of the Zry cladding looses its protective character to a large extent during the quench process. The protective ZrO_2 layer, growing during heatup, reduces the oxidation reaction reciprocally to the layer thickness. Spallations or cracks caused by the quench process would allow the access of the increased steam to hot metallic Zry. The Zr/steam reaction, growing exponentially with temperature can result in the measured temperature escalation, in parallel to the corresponding hydrogen production.
But to be able to describe the quench process in SFD computer codes, it is necesssary to understand the mechanisms in detail, so that they could be described in a quantative way. Therefore further experiments are necessary. The

construction of a new bundle quench facility is under way at the Forschungszentrum Karlsruhe.

5. References

/1/ S. Hagen, K. Hain, "Out-of-pile Bundle Experiments on Severe Fuel Damage (CORA-Program): Objectives, Test Matrix and Facility Description", KfK 3677 (1986).

/2/ A.D. Knipe, S.A. Ploger, D.J. Osetek, "PBF Severe Fuel Damage Scoping Test - Test Results Report", NUREG/CR-4683, U.S. Nuclear Regulatory Commission (March 1996).

/3/ S. Hagen, P. Hofmann, G. Schanz, L. Sepold, "Interactions in Zry/UO_2 Fuel Rod Bundles with Inconel Spacers at Temperatures above 1200°C; (Posttest Results of Severe Fuel Damage Experiments CORA-2 and CORA-3)", KfK 4378 (1990).

/4/ S. Hagen, V. Noack, L. Sepold, P. Hofmann, G. Schanz, G. Schumacher, "Results of SFD Experiments CORA-13 (OECD International Standard Problem 31)", KfK 5054 (1993).

/5/ M. Firnhaber, K. Trambauer, S. Hagen, P. Hofmann, "ISP-31 OECD/NEA-CSNI International Standard Problem, CORA-13 Experiment on Severe Fuel Damage, NEA/CSNI/R (93) 17, GRS-106, KfK 5287 (1993)

/6/ J. Burbach, "Ergebnisse von REM-Mikrobereichsanalysen des DWR-Bündelabschmelzexperimentes CORA-13" KfK 5162 (1993).

/7/ J. Burbach, "Ergebnisse von REM/EDX-Mikrobereichsanalysen des SWR-Bündelabschmelzexperimentes CORA-16, KfK 4560 (1994).

/8/ S. Hagen, P. Hofmann, V. Noack, G. Schanz. G. Schumacher, L. Sepold; "Dry Core BWR Test CORA-33: Test Results", KfK 5261 (1994).

/9/ L. Belovsky, IAEA TCM on "Behaviour of LWR Core Material under Accident Conditions". Oct. 9-13, 1995 Dimitrovgrad, Russia.

/10/ S. Hagen, F. Seibert, L. Sepold., P. Hofmann, G. Schanz, G. Schumacher, "Influence of Reflood in the CORA Severe Fuel Damage Experiments", Heat Transfer and Fuel Behaviour in Nuclear Reactor Accidents, 27th ASME/AIChE/ANS National Heat Transfer Conference, Minneapolis, 28-31July 1991, AIChE Symposium Series 283, Vol. 87 ISBN-0-8169-0548-7, pp. 120-129

6. Acknowledgements

We gratefully appreciate the thorough and critical review of this paper by Dr. T. Haste of AEA Technology, Winfrith.

At the Forschungszentrum Karlsruhe support in many fields needed for preparation, conduct, and evaluation of the experiments is hereby gratefully acknowledged.

The facility was designed by K. Hain and his team. The special bundle setup was arranged by Mr. H. Junker. The test rods were assembled by Mr. E. Mackert, the

test bundles by Messrs. H. Gießmann and R. Röder. The authors would like to thank Messrs. H. Benz, C. Grehl and H.J. Röhling for test preparations and conduct.

Mr. K.P. Wallenfels was responsible for arrangement of camera and video systems and for the preparation of temperature measurements. Messrs. R. Huber and H. Malauschek prepared and conducted the on-line measurements of the off-gas composition. We thank Mr. L. Anselment for sectioning of the epoxied bundle and for the preparation of the metallographic samples, Mr. H. Metzger for examination of the metallographic samples by optical microscope, and Mr. J. Burbach for the SEM examinations.

We would like finally to express our gratitude to Mrs. U. Ivanitsch for the careful typing of this report.

7. List of Tables

Tab. 1: CORA Test Matrix

Test No.	Max. Cladding Tempera-tures	Absorber Material	Other Test Conditions	Date of Test
2	≈ 2000°C	-	UO_2 refer., inconel spacer	Aug. 6, 1987
3	≈ 2400°C	-	UO_2 refer., high temperature	Dec. 3, 1987
5	≈ 2000°C	Ag, In, Cd	PWR-absorber	Febr. 26, 1988
12	≈ 2000°C	Ag, In, Cd	quenching	June 9, 1988
16	≈ 2000°C	B_4C	BWR-absorber	Nov. 24, 1988
15	≈ 2000°C	Ag, In, Cd	rods with internal pressure	March 2, 1989
17	≈ 2000°C	B_4C	quenching	June 29, 1989
9	≈ 2000°C	Ag, In, Cd	10 bar system pressure	Nov. 9, 1989
7	< 2000°C	Ag, In ,Cd	57-rod bundle, slow cooling	Febr. 22, 1990
18	< 2000°C	B_4C	59-rod bundle, slow cooling	June 21, 1990
13	≈ 2200°C	Ag, In, Cd	OECD/ISP; quench initiation at higher temperature	Nov. 15, 1990
29*	≈ 2000°C	Ag, In, Cd	pre-oxidized,	April 11, 1991
31*	≈ 2000°C	B_4C	slow initial heat-up (≈ 0.3 K/s)	July 25, 1991
30*	≈ 2000°C	Ag, In, Cd	slow initial heat-up (≈ 0.2 K/s)	Oct. 30, 1991
28*	≈ 2000°C	B_4C	pre-oxidized	Febr. 25, 1992
10	≈ 2000°C	Ag, In, Cd	cold lower end 2 g/s steam flow rate	July 16, 1992
33	≈ 2000°C	B_4C	dry core conditions, no extra steam input	Oct. 1, 1992
W1	≈ 2000°C	-	WWER-test	Febr. 18, 1993
W2	≈ 2000°C	B_4C	WWER-test with absorber	April 21, 1993

Initial heat-up rate: ≈ 1,0 K/s; Steam flow rate, PWR: 6 g/s, BWR: 2 g/s; quench rate (from the bottom) ≈ 1 cm/s

Tab.2: Design characteristics of the PWR bundle

Bundle type:		PWR
Bundle size:		25 rods
Number of heated rods:		16
Number of unheated rods:		7
Pitch:		14.3 mm
Rod outside diameter:		10.75 mm
Cladding material:		Zircaloy-4
Cladding thickness:		0.725 mm
Rod length:	- heated rods: (elevation	1960 mm - 489 to 1471 mm)
	- unheated rods (elevation	1672 mm - 201 to 1471 mm)
Heated pellet stack:		1000 mm
Heater material:		Tungsten (W)
Heater	- length	1000 mm
	- diameter	6 mm
Fuel pellets	- heated rods:	UO_2 annular pellets
	- unheated rods:	UO_2 full pellets
Pellet stack	- heated rods: - unheated rods:	O to 1000 mm - 199 to 1295 mm
U-235 enrichment		0.2 %
Pellet outer diameter (nominal)		9.1 mm
Grid spacer	- material:	Zircaloy -4, Inconel 718
	- length:	Zry 42 mm Inc 38 mm
	- location:	lower (Zry) -5 mm center (Inc) +496 mm top (Zry) +880 mm
Shroud	- material	Zircaloy -4
	- wall thickness	1.2 mm
	- outside dimensions ·	89.4 x 90.4 mm
	- elevation	36 mm to 1231 mm
Shroud insulation		ZrO_2 fibre
	- insulation thickness	19 mm
	- elevation	36 mm to 1036 mm

Tab.2: (Continuation)

Mo electrode	- length	300 mm
	- diameter	8,6 mm
Cu electrode	- length	189 mm (lower end)
	- length	669 mm (upper end)
	- diameter	8,6 mm
Absorber rod	- number of rods	2
	- material and composition	80Ag,15In,5Cd (wt.%)
	- cladding	Stainless steel
	- cladding OD	11,2 mm
	- cladding ID	10,2 mm
	- length	1660 mm
	- absorber material	-189 mm to +1300 mm
Absorber rod guide tube	- material	Zircaloy -4
	- OD	13,8 mm
	- wall thickness of tube	0,8 mm
Plenum Volume	- heated rods	$12 \cdot 10^{-6}$ m^3
	- unheated rods	$87 \cdot 10^{-6}$ m^3

Tab.3: Design characteristics of the BWR bundle

Bundle type		BWR
Bundle size		18 rods
Number of heated rods		12
Number of unheated rods		6
Pitch		14.3 mm
Rod outside diameter		10.75 mm
Cladding material		Zircaloy-4
Cladding thickness		0.725 mm
Rod length	- heated rods elevation	1840 mm - 369 to 1471 mm
	- unheated rods elevation	1672 mm - 201 to 1471 mm
Heated pellet stack		0 to 1000 mm
Heater material		Tungsten (W)
Heater	- length	1000 mm
	- diameter	6 mm
Fuel pellets	- heated rods	UO_2 annular pellets
	- unheated rods	UO_2 full pellets
Pellet stack	- heated rods	0 to 1000 mm
	- unheated rods:	- 200 to 1300 mm
U-235 enrichment		0.2 %
Pellet outer diameter (nominal)		9.1 mm
Grid spacer	- material	Zircaloy -4
	- length	42 mm
	- location (upper end)	lower -33 mm center 578 mm top 1167 mm
Shroud	- material	Zircaloy -4
	- wall thickness	1.2 mm
	- outside dimensions	94.4 x 116 mm
	- elevation	40 - 1235 mm

Tab.3: (Continuation)

Shroud insulation	- material	ZrO_2 fibre
	- thickness of insulation	19 mm
	- elevation	40 mm to 1110 mm
Mo electrode	- length	300 mm (upper and lower ends, resp.)
	- diameter	8.6 mm
Cu electrode	- length	189 mm (lower end)
	- length	669 mm (upper end)
	- diameter	8.6 mm
Absorber rod	- number of rods	11
	- material	B_4C powder
	- cladding	stainless steel
	- cladding OD	5.8 mm
	- cladding ID	4.6 mm
	- length	1600 mm
	- absorber material	-270 mm to +1300 mm
Absorber blade	- material	stainless steel
	- inside dimensions	76 x 6 mm
	- wall thickness	1 mm
Channel box wall	- material	Zircaloy -4
	- inside dimensions	13 x 92 mm
	- wall thickness	1.2 mm
Plenum Volume	- heated rods	$19.8 \cdot 10^{-6}$ m^3
	- unheated rods	$39.0 \cdot 10^{-6}$ m^3

9. List of Figures

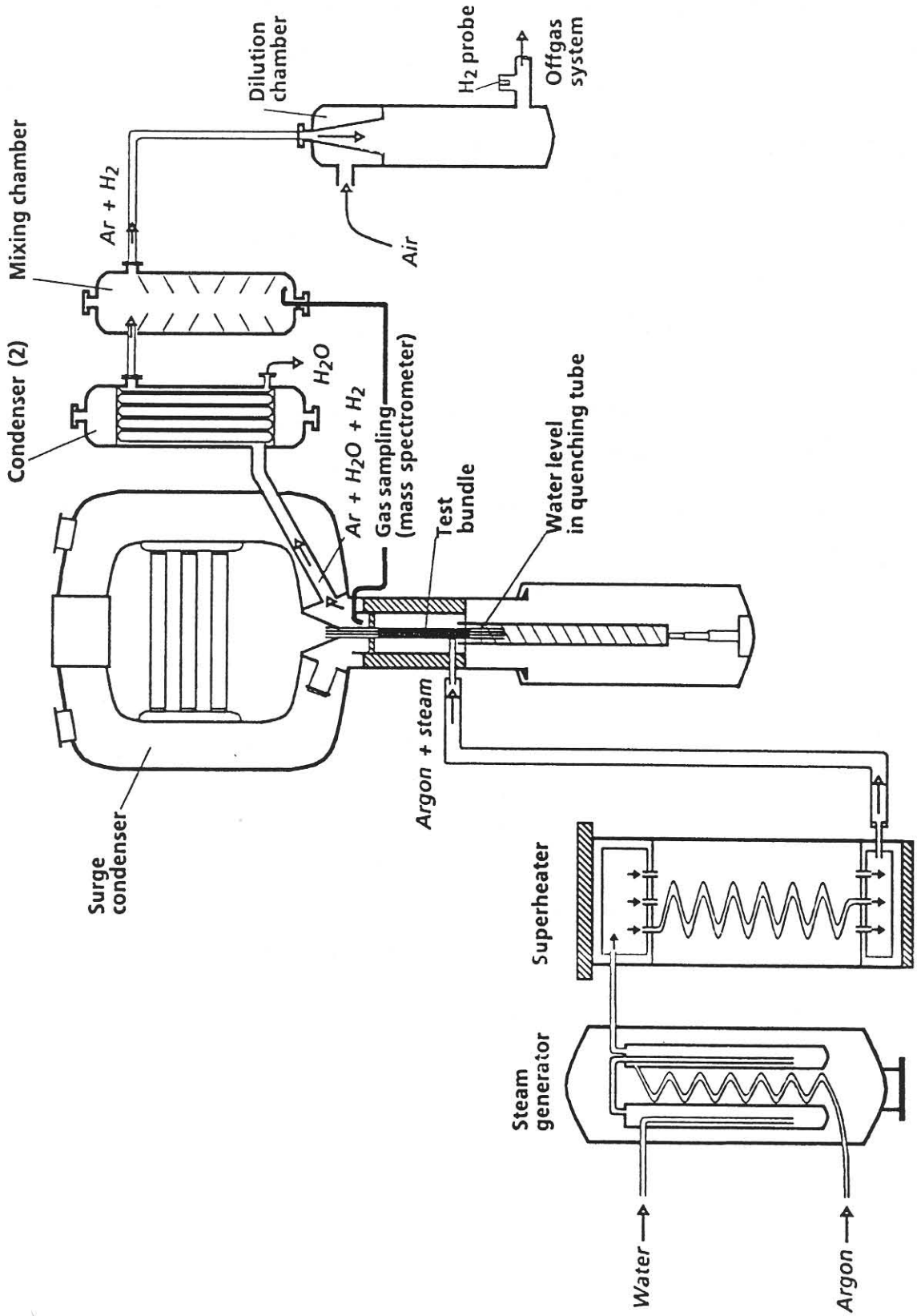

Fig. 1: Simplified flow diagram of the CORA facility

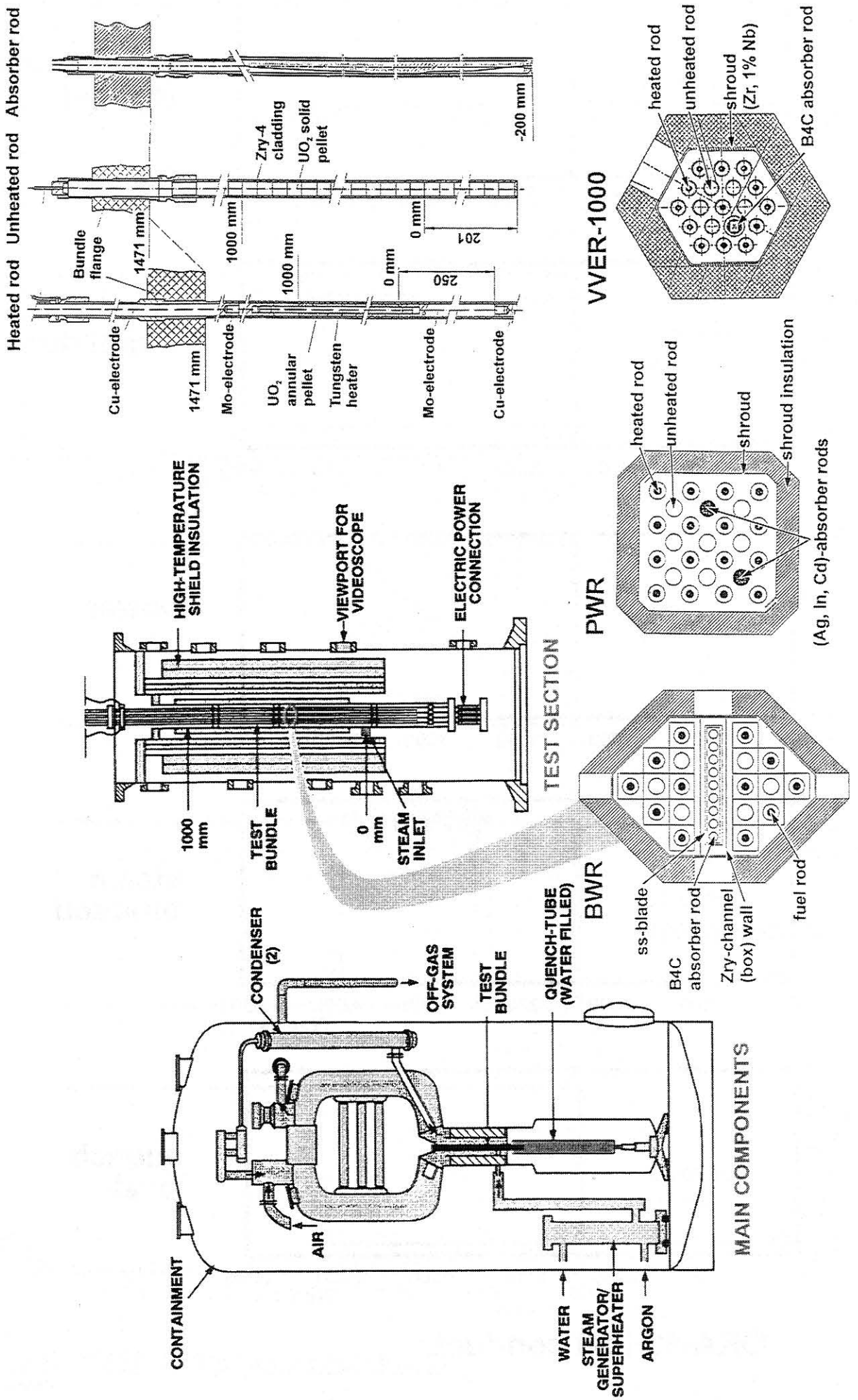

Fig.2: CORA Severe Fuel Damage Test Facility

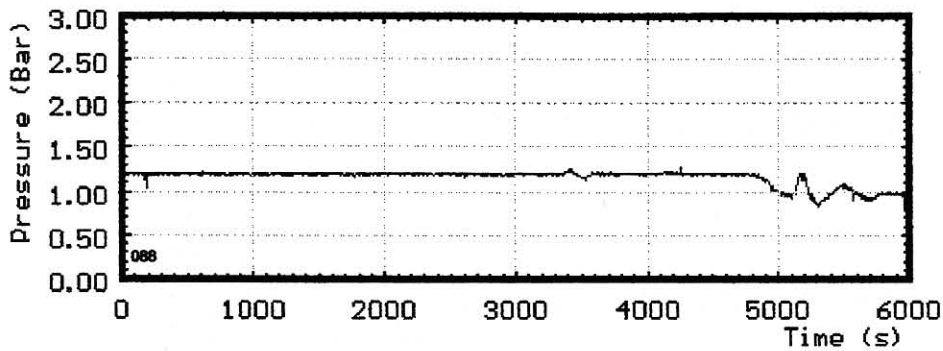

system pressure (gauge)

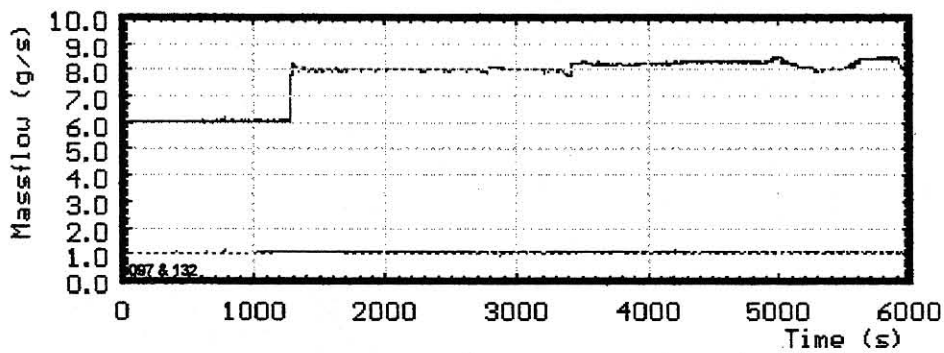

argon flow

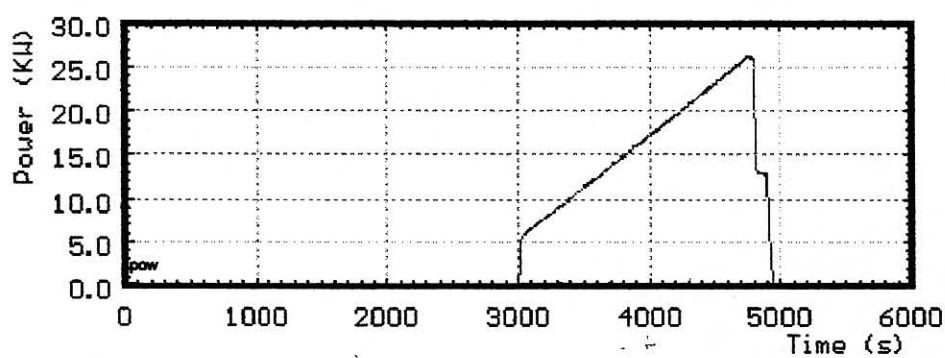

power

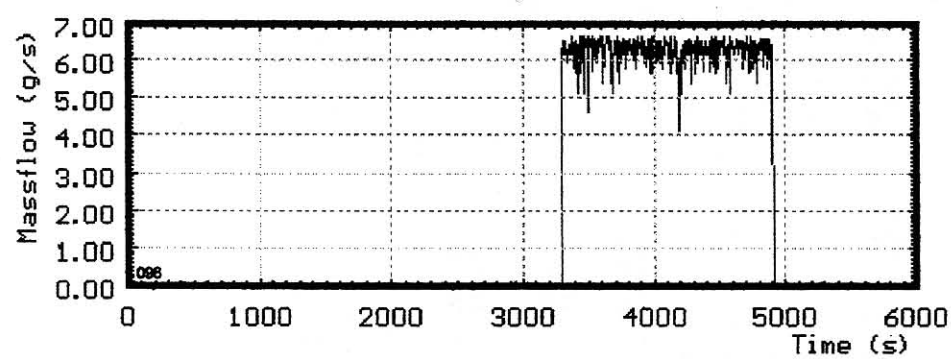

steam production

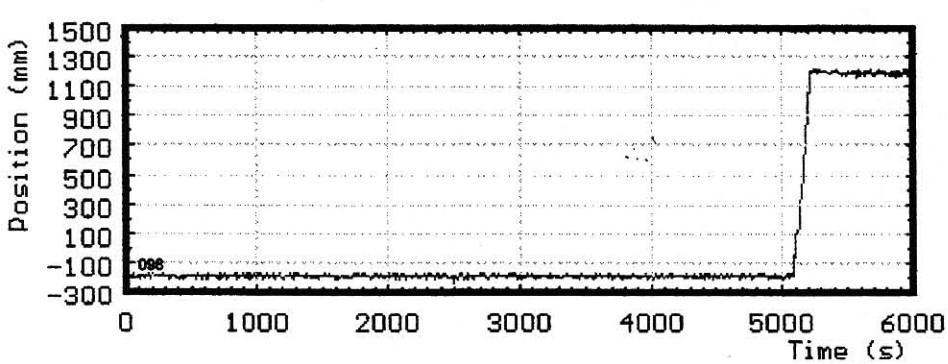

quench level

Fig.3: CORA-12 test conduct.

C12\c12_conq.cdr

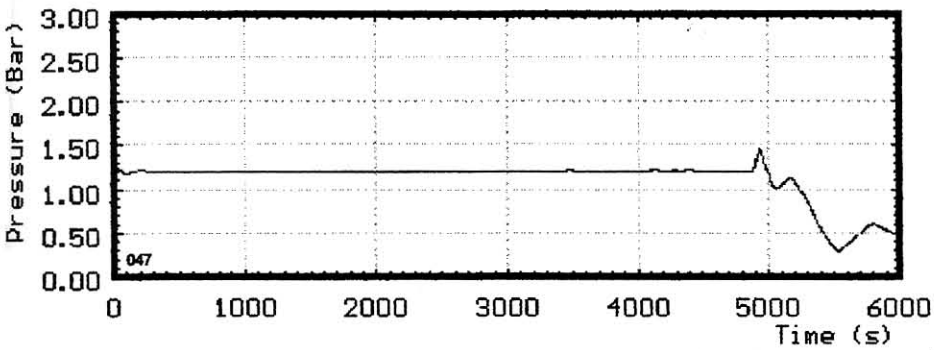

system pressure (gauge)

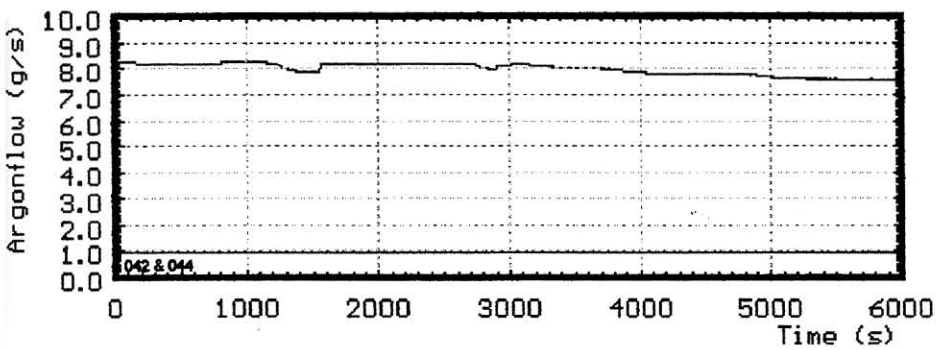

argon flow

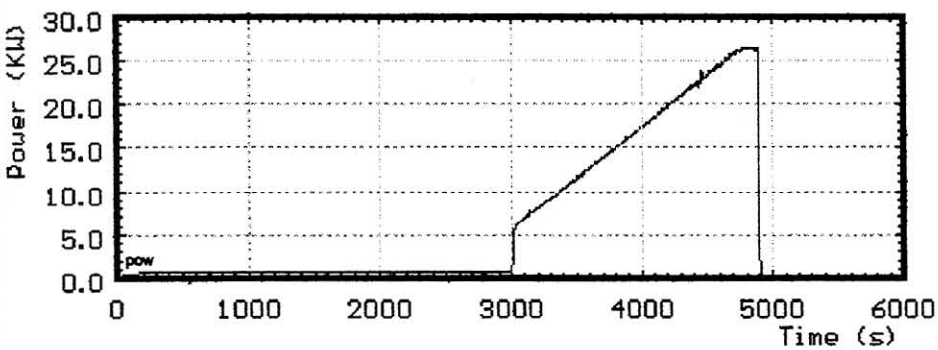

power

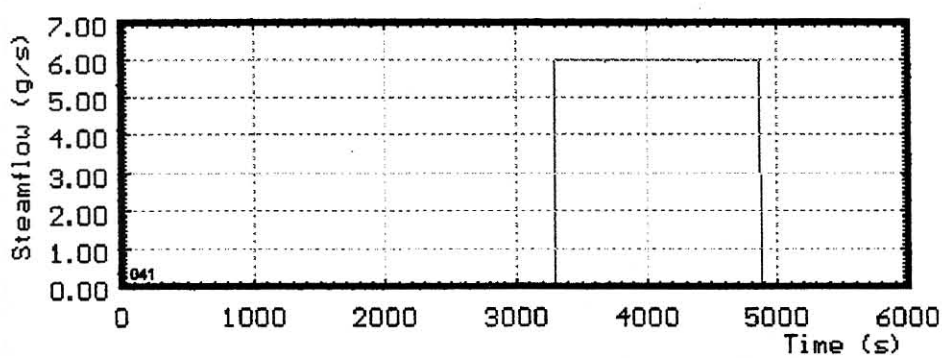

steam production

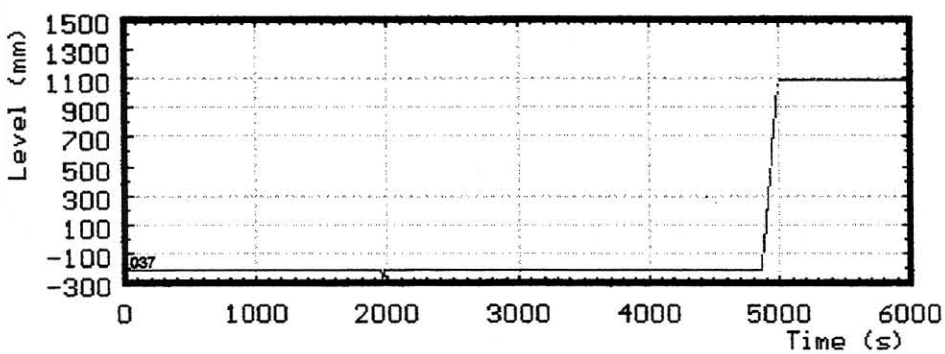

quench level

Fig.4: CORA-13 test conduct.

C13\c13_conq.cdr

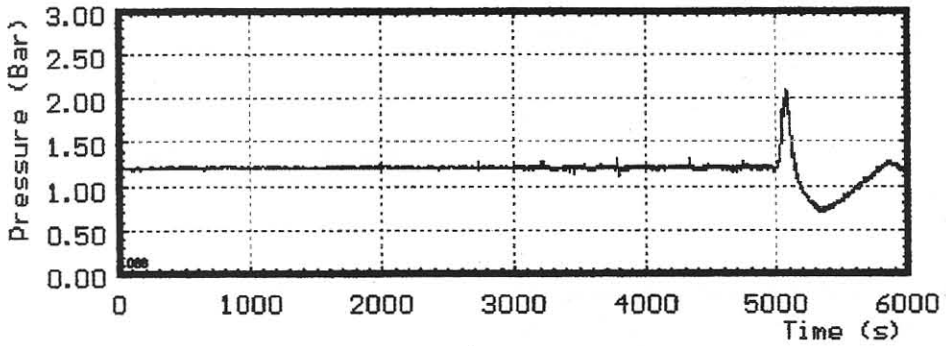

system pressure (gauge)

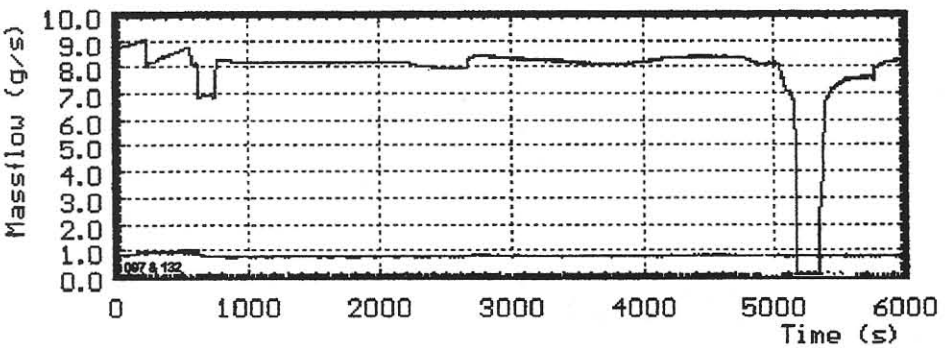

argon flow

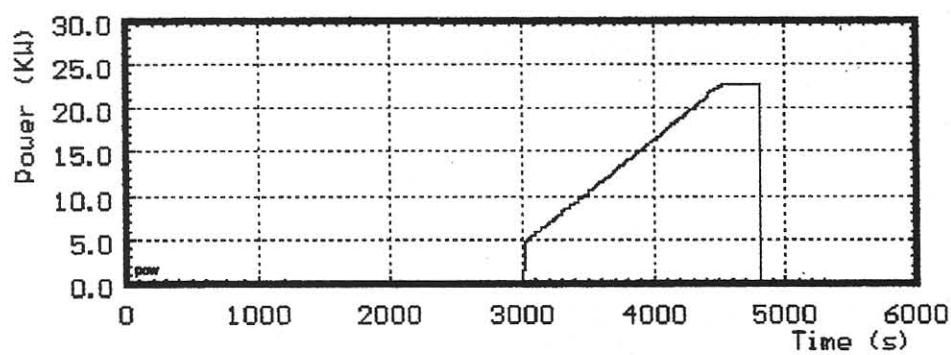

power

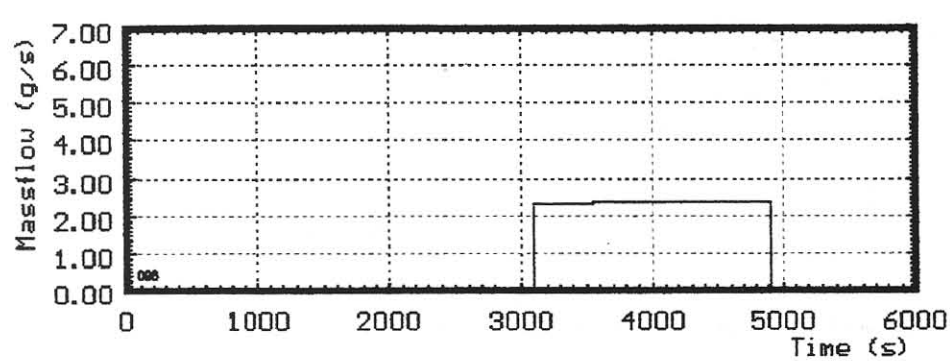

steam production

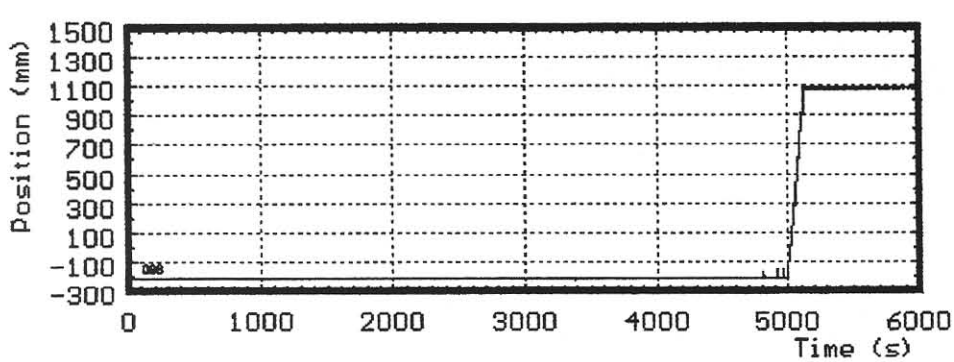

quench level

Fig.5: CORA-17 test conduct.

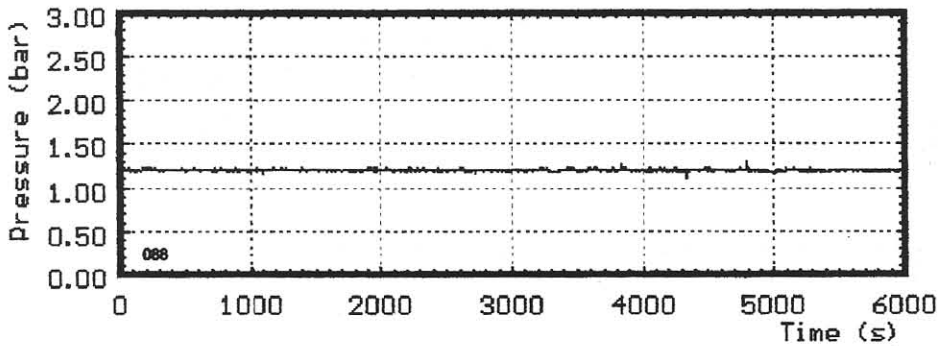

system pressure (gauge)

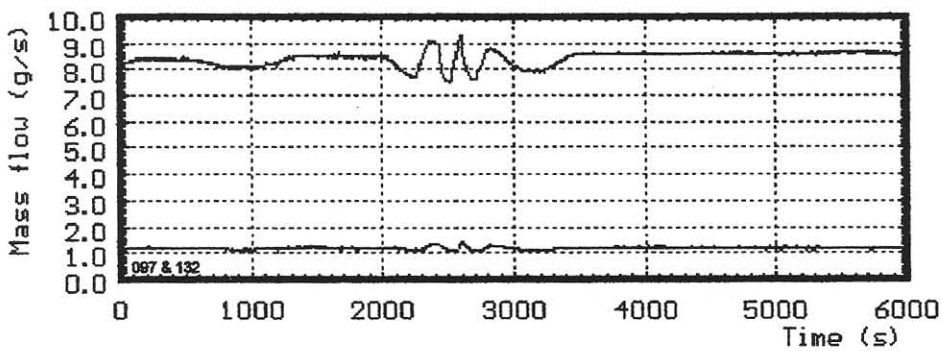

argon flow

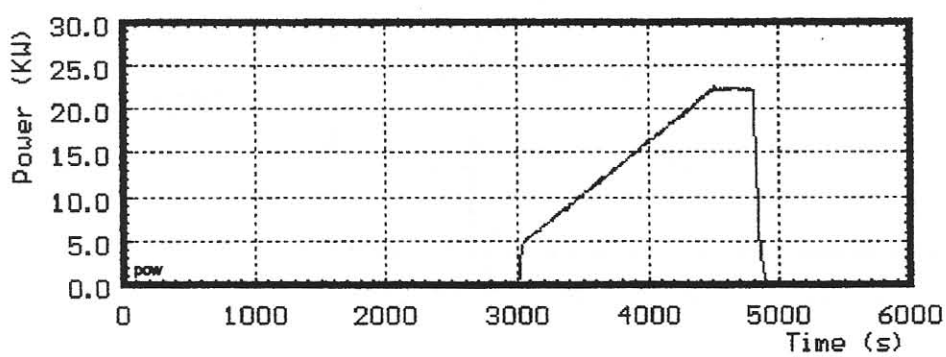

power

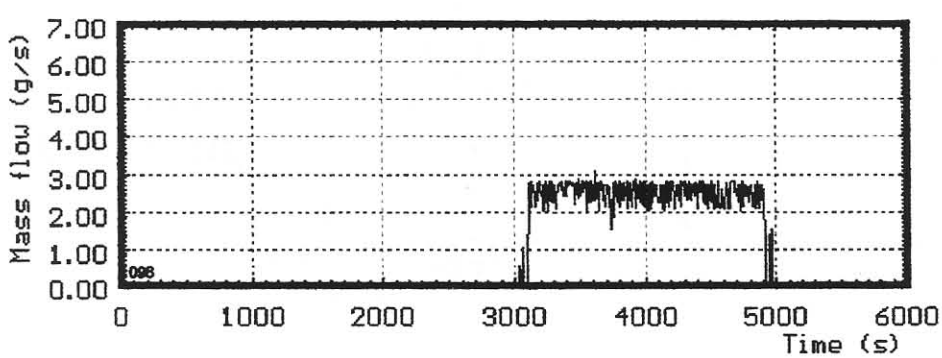

steam production

no quenching

Fig.6: CORA-16 test conduct.

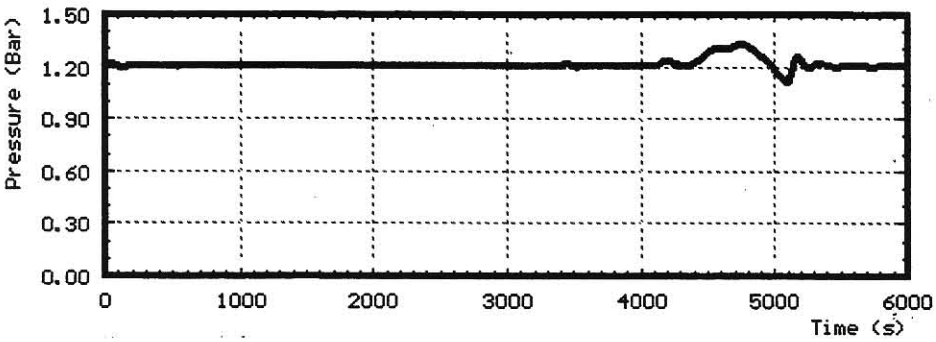

system pressure (gauge)

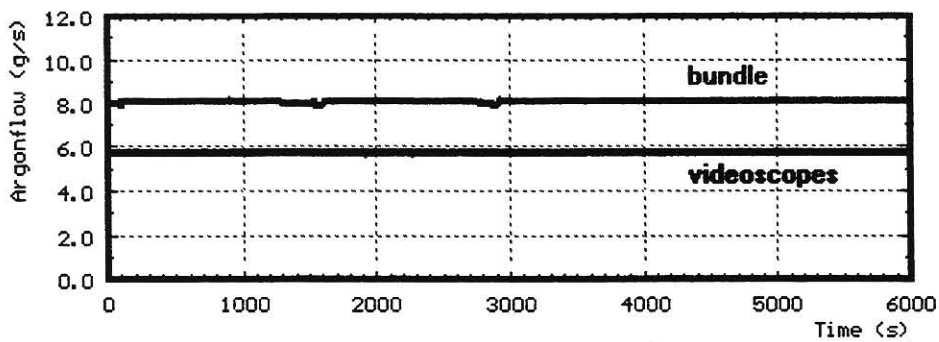

argon flow

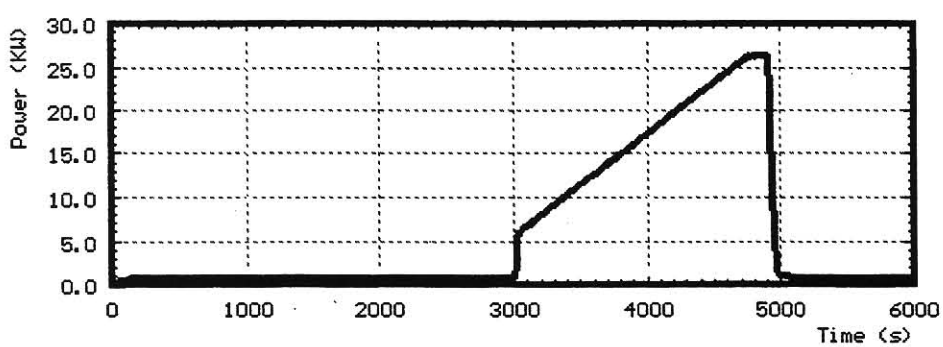

power

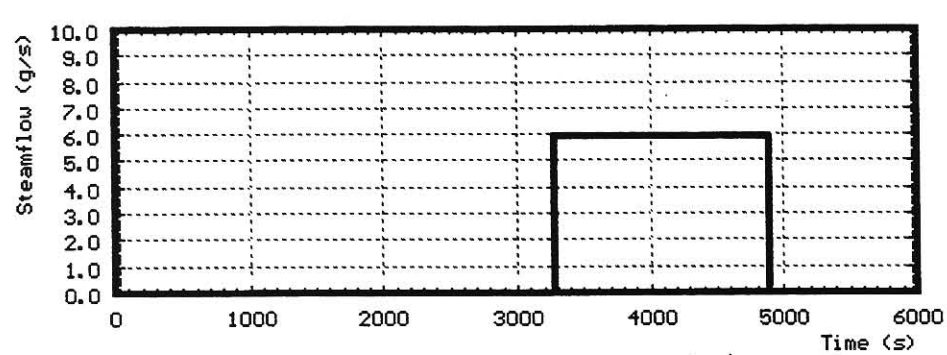

steam production

no quenching

Fig.7: CORA-29 test conduct.

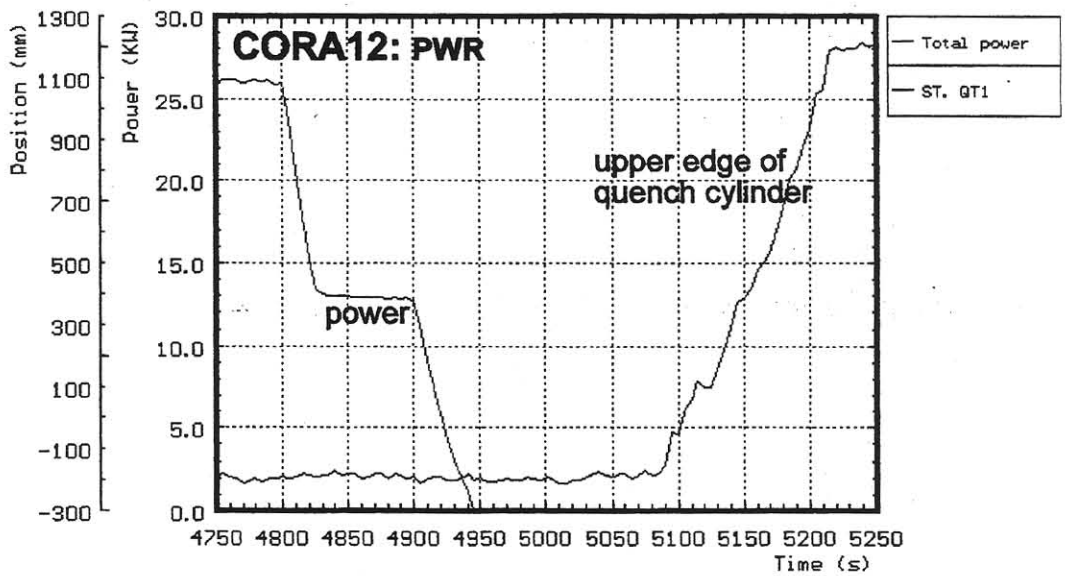

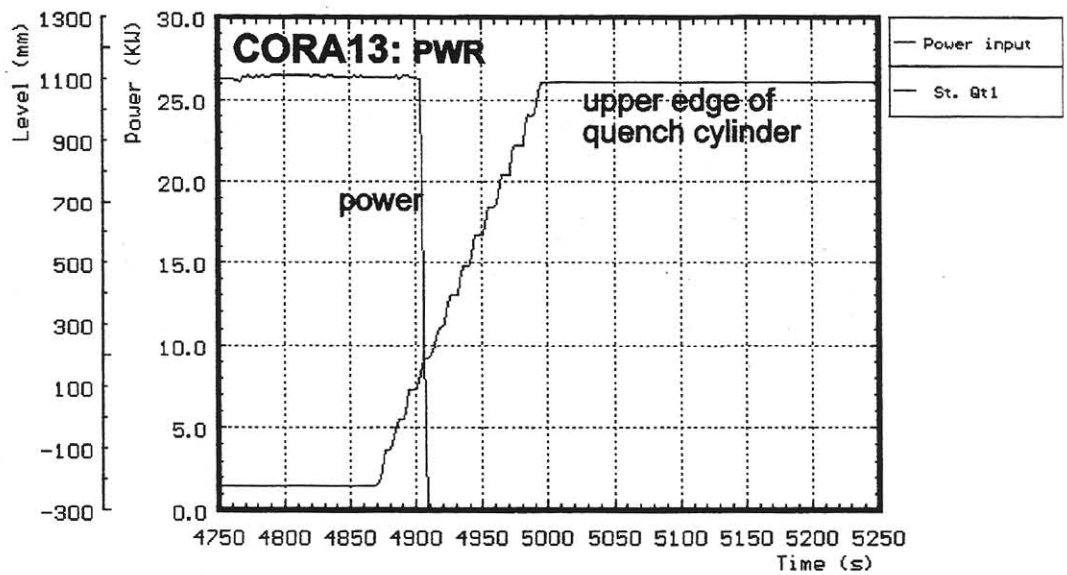

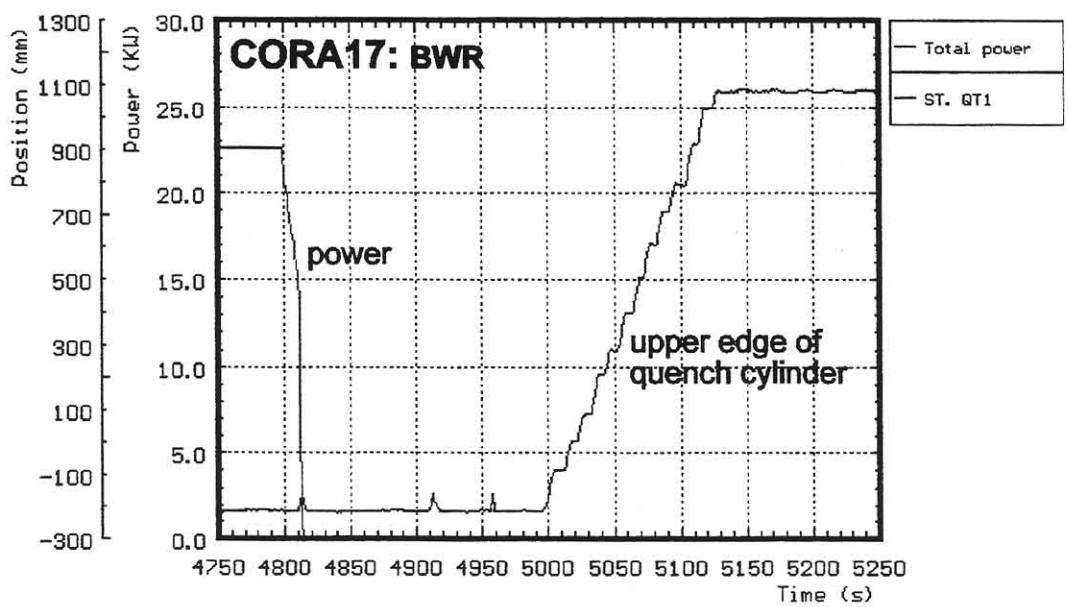

Fig.8: Axial movement of upper edge of quench cylinder compared to the power input

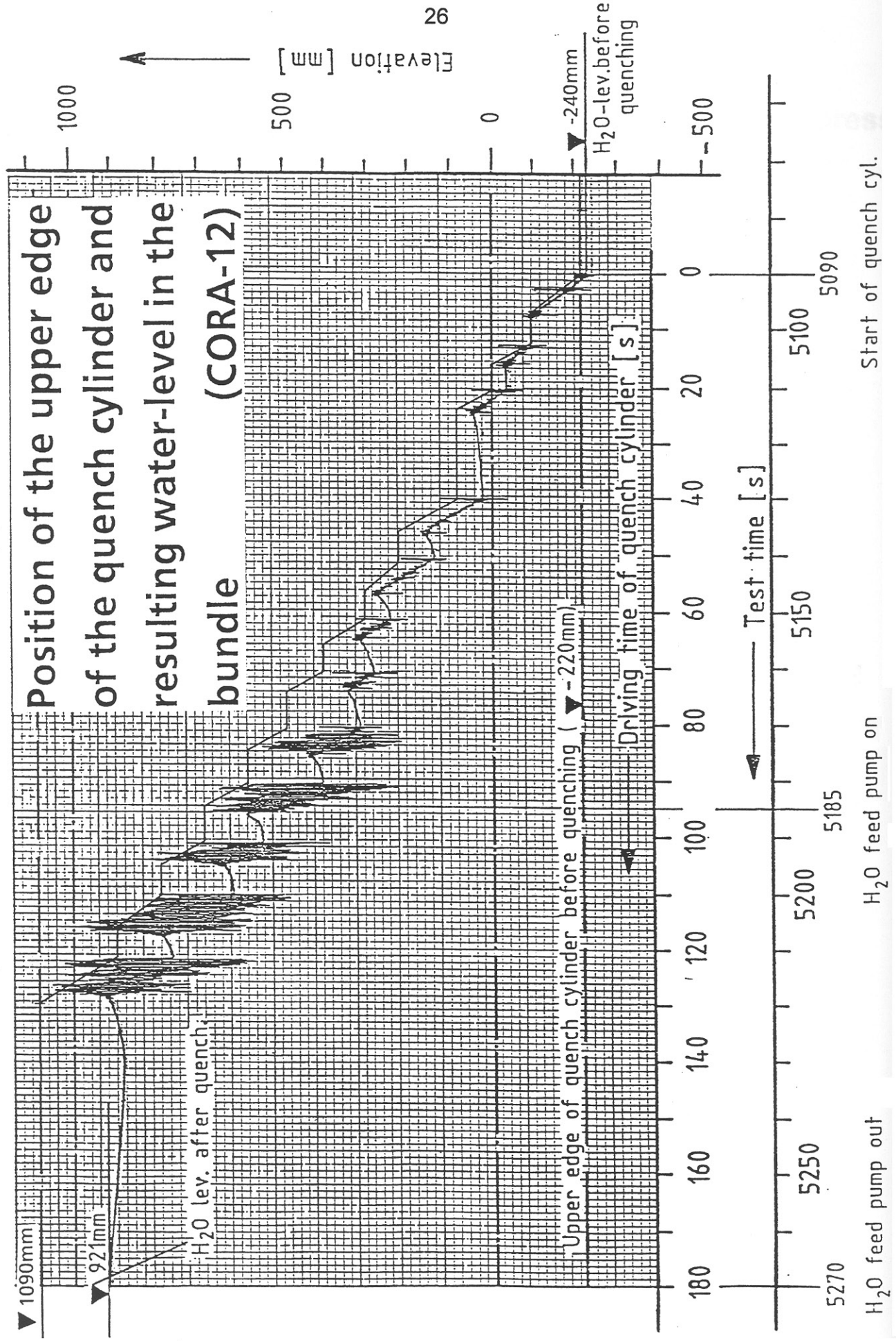

Fig.9: Position of the upper edge of the quench cylinder and resulting water-level in the bundle (CORA-12: PWR)

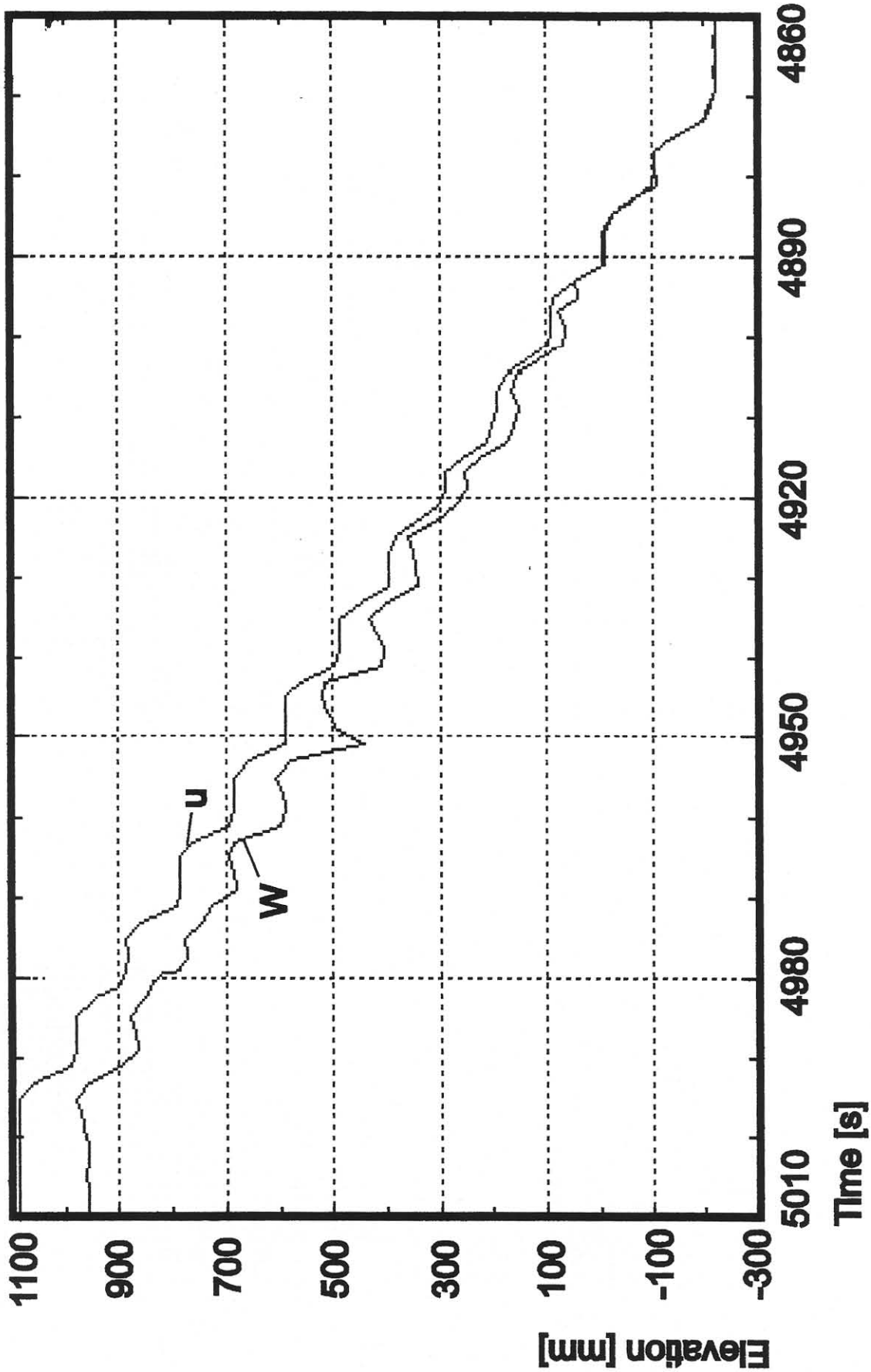

Fig.10: Position of the upper edge of the quench cylinder and resulting water level in the bundle of CORA-13

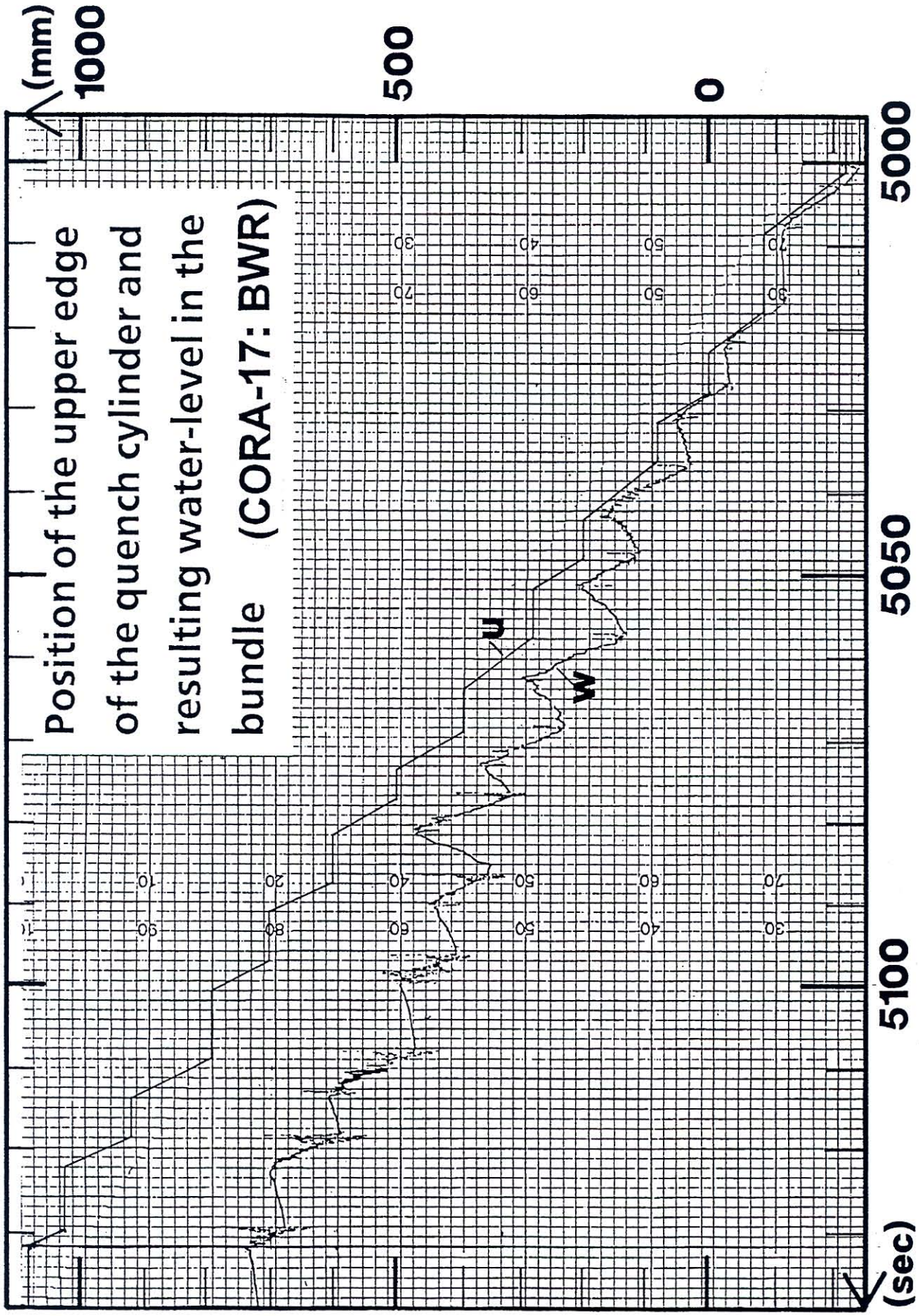

Fig.11: Position of the upper edge of the quench cylinder and resulting water-level in the bundle **(CORA-17: BWR)**

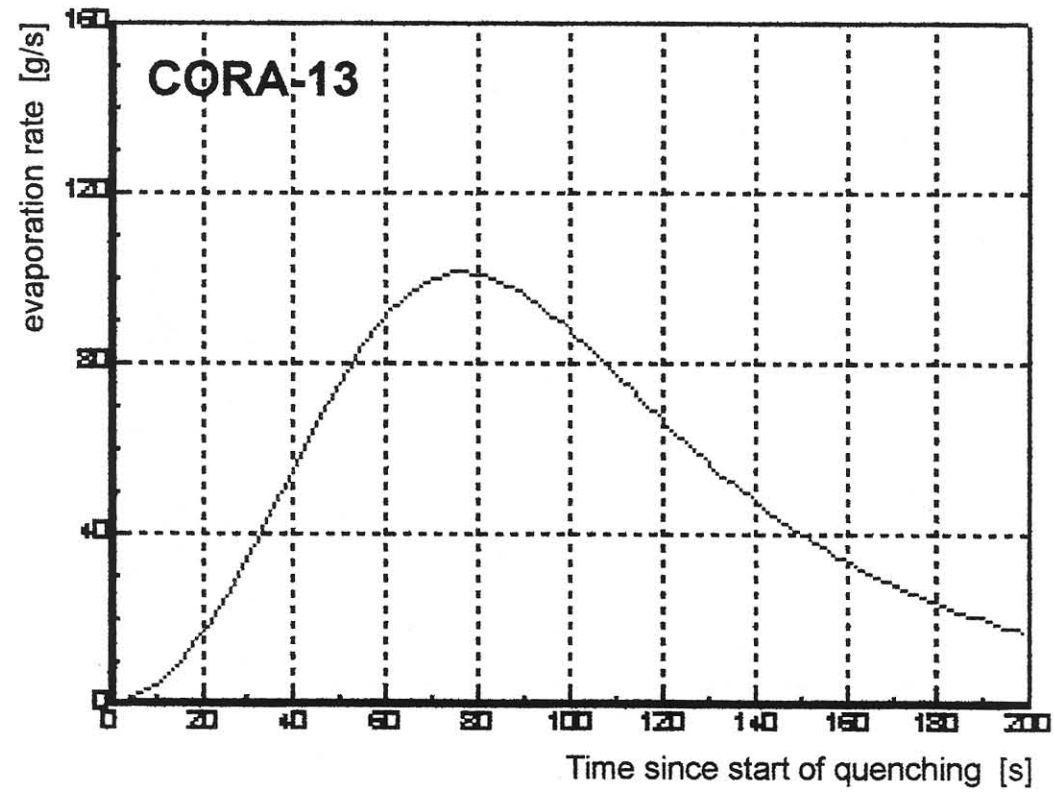

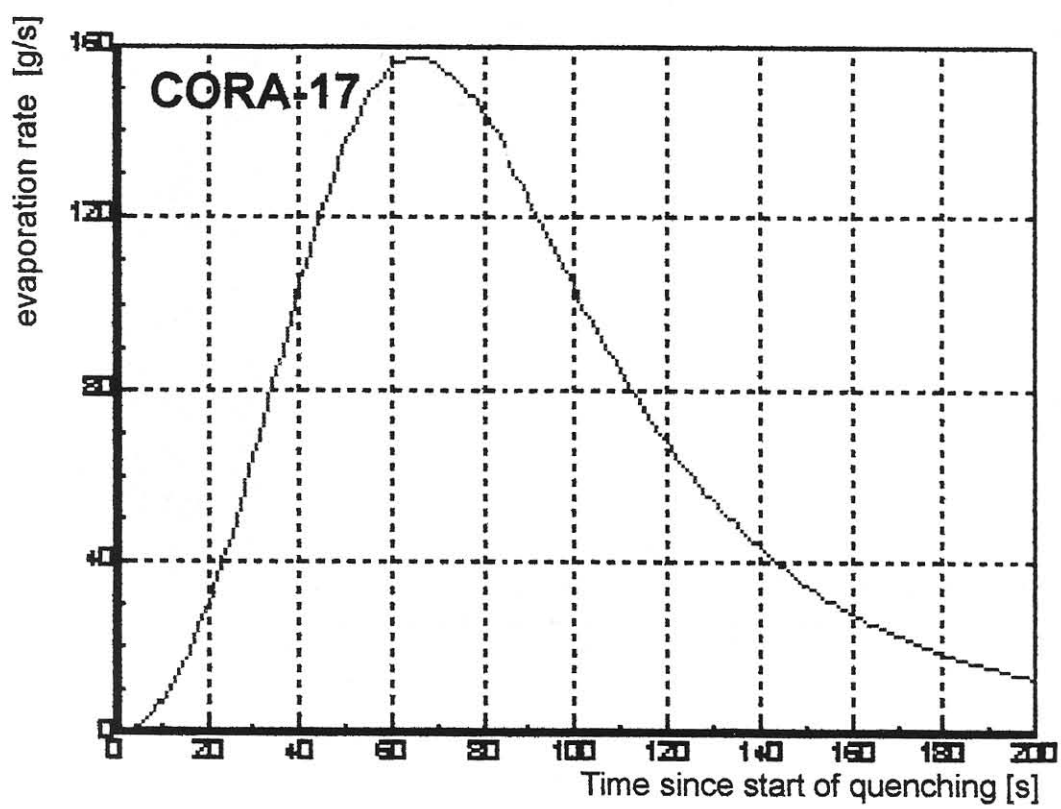

Fig.12: Evaporation rate (g/s) during the quench process

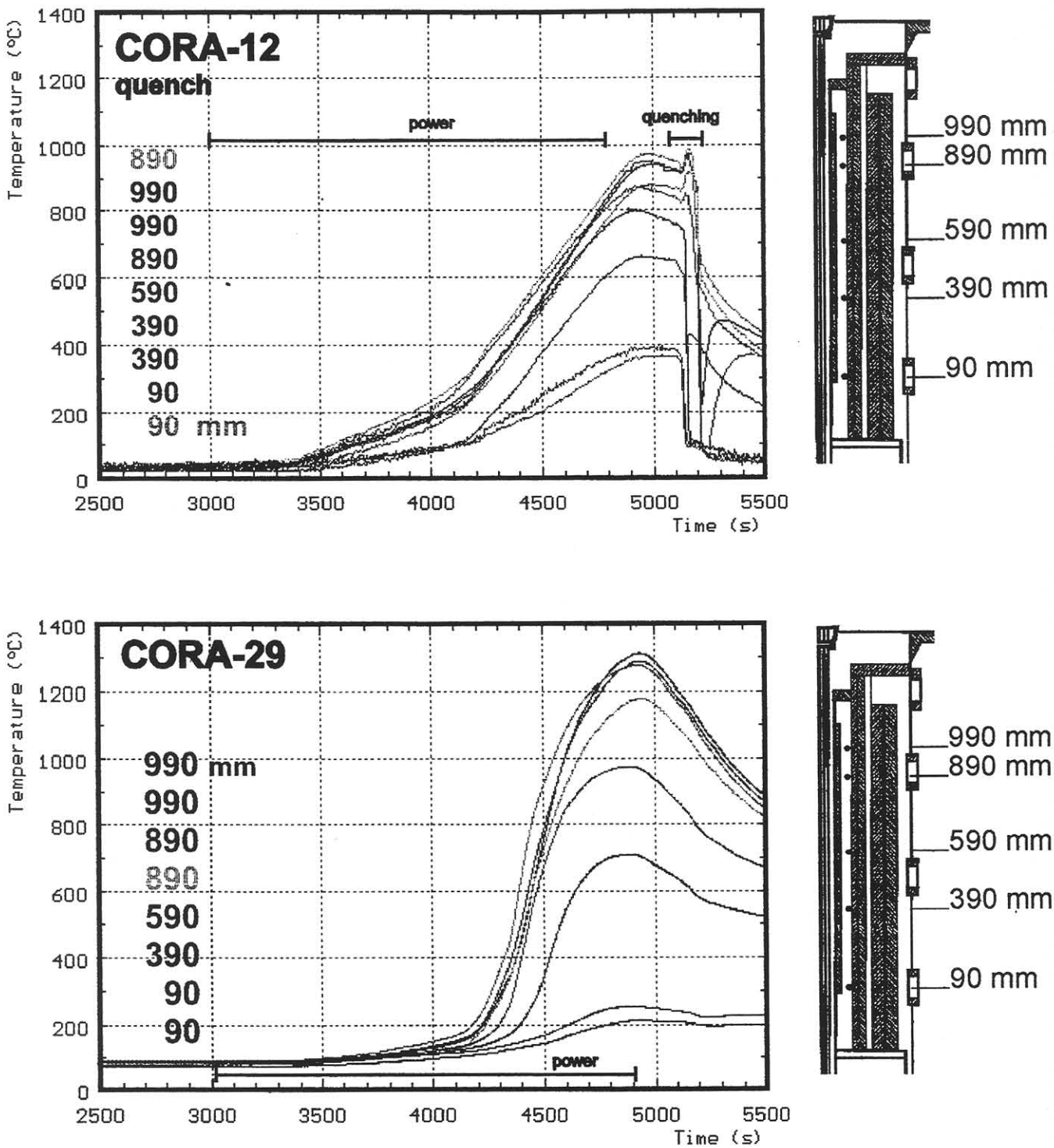

Fig.13: Comparsion of the temperatures at the inner wall of the HTS for tests CORA-12 / CORA-29 (PWR).

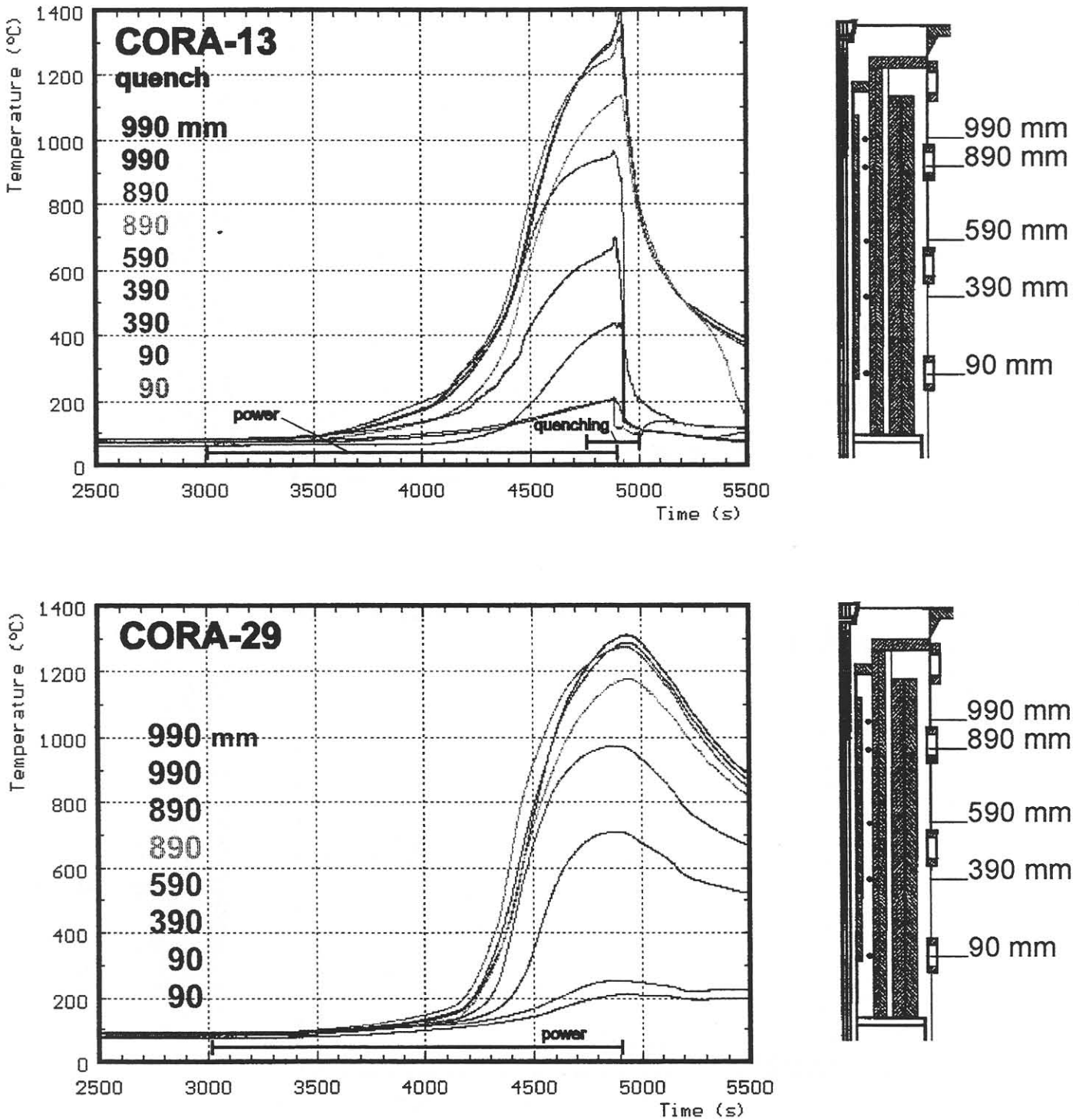

Fig.14: Comparsion of the temperatures at the inner wall of the HTS for tests CORA-13 / CORA-29 (PWR).

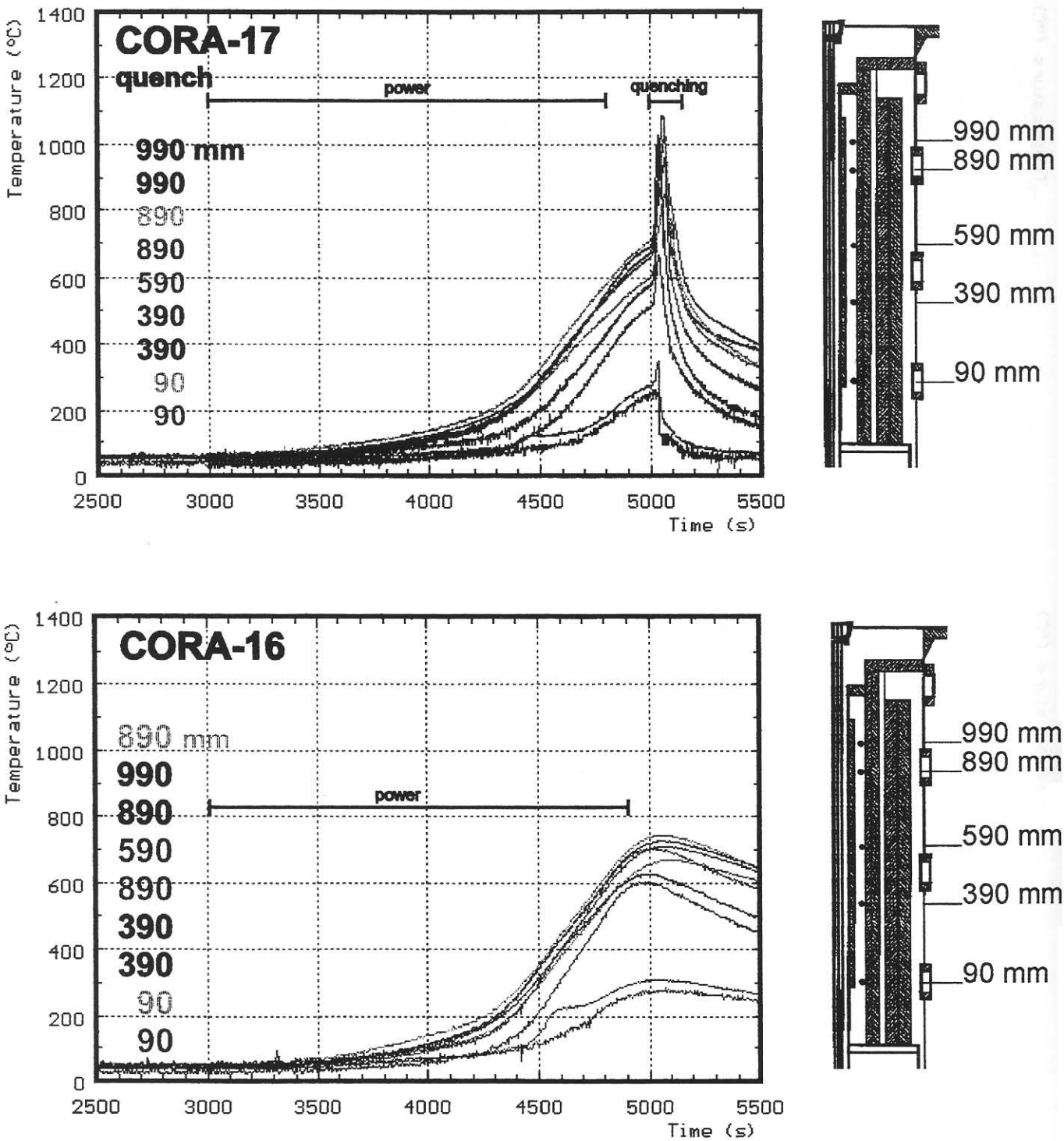

Fig.15: Comparsion of the temperatures at the inner wall of the HTS for tests CORA-17 / CORA-16 (BWR).

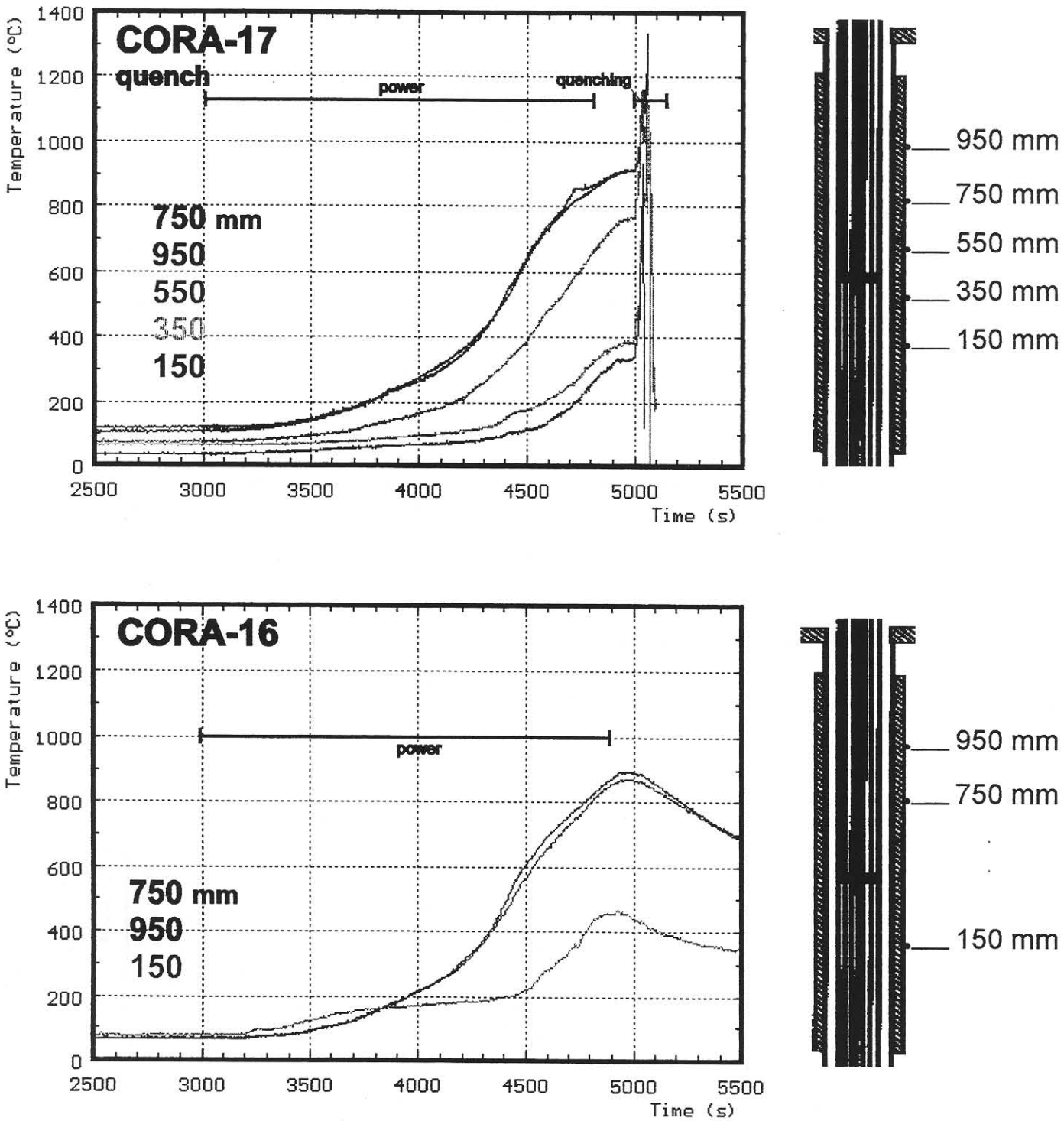

Fig.16: Comparsion of the temperatures at the shroud insulation for tests CORA-17 / CORA-16 (BWR).

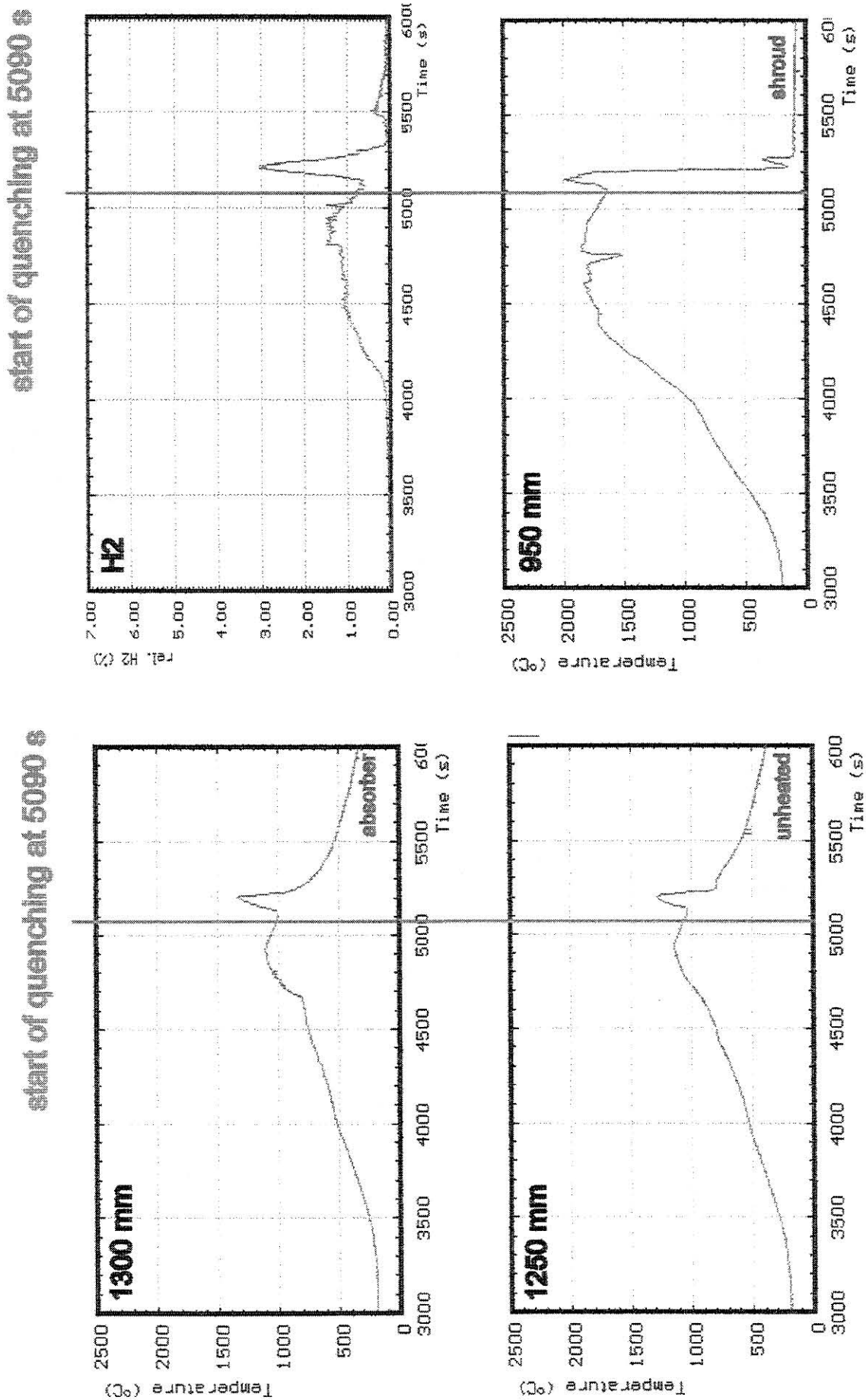

Fig.17: Temperature peaks and hydrogen production due to quenching of CORA-12

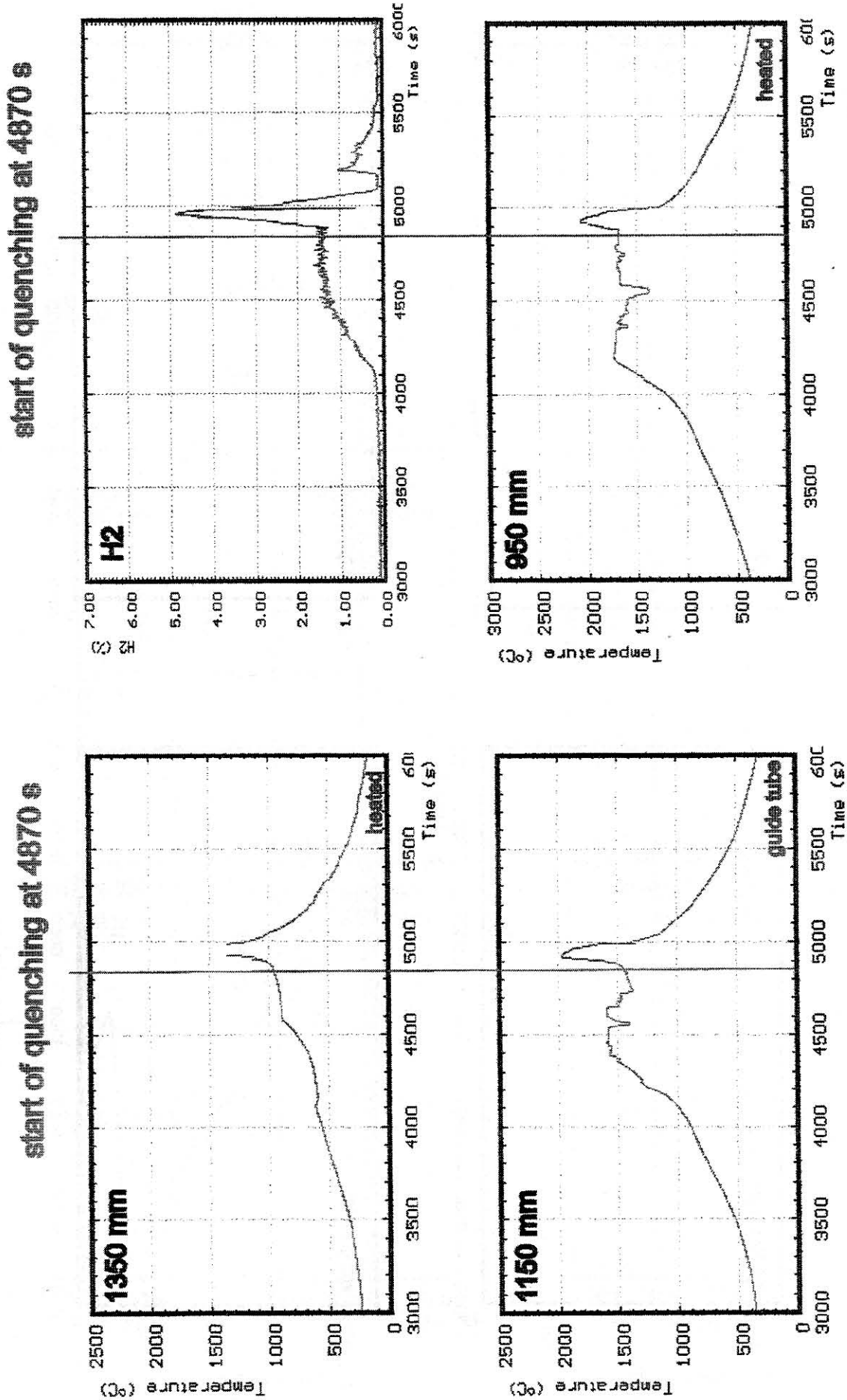

Fig.18: Temperature peaks and hydrogen production due to quenching of CORA-13

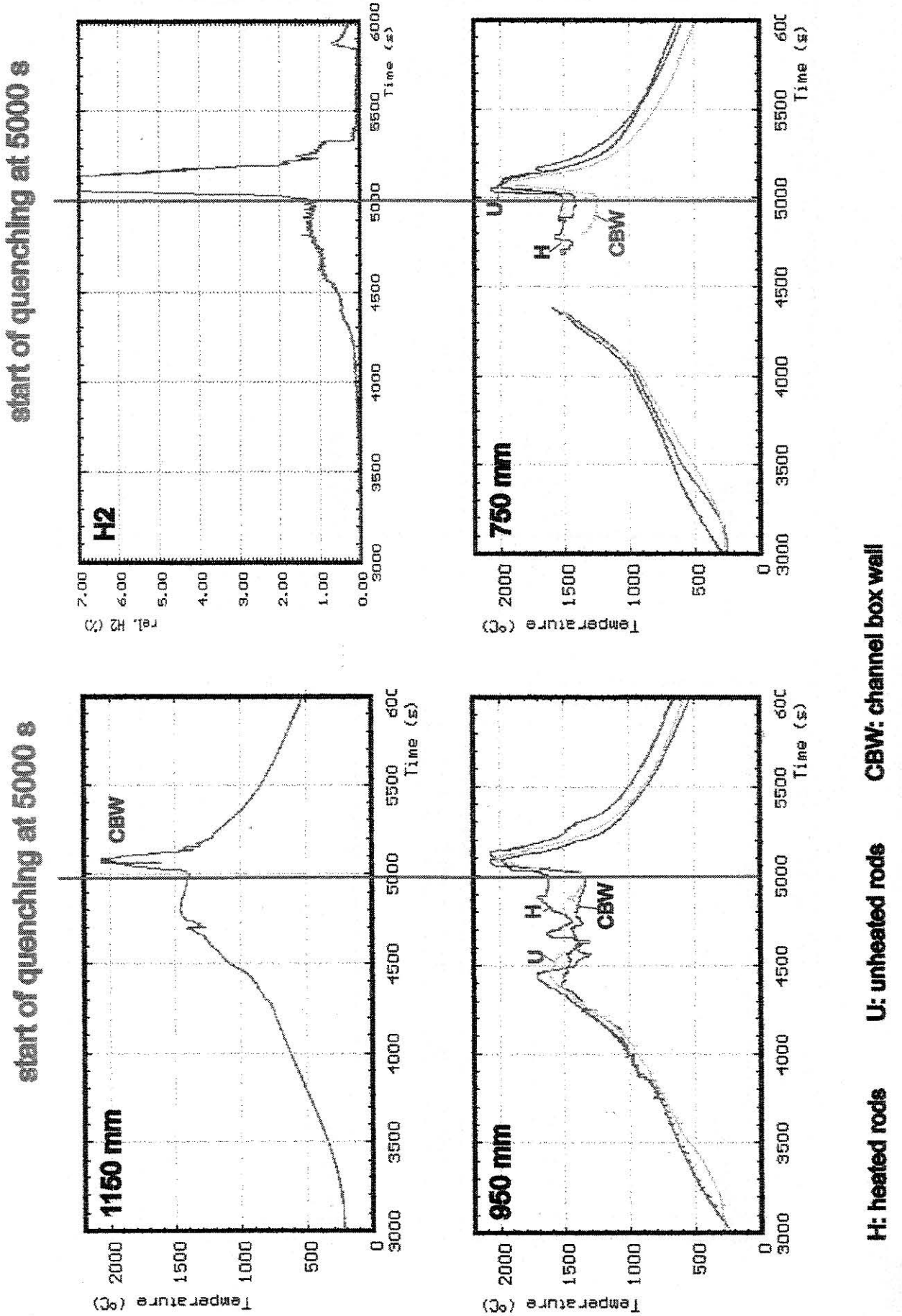

Fig.19: Temperature peaks and hydrogen production due to quenching of CORA-17

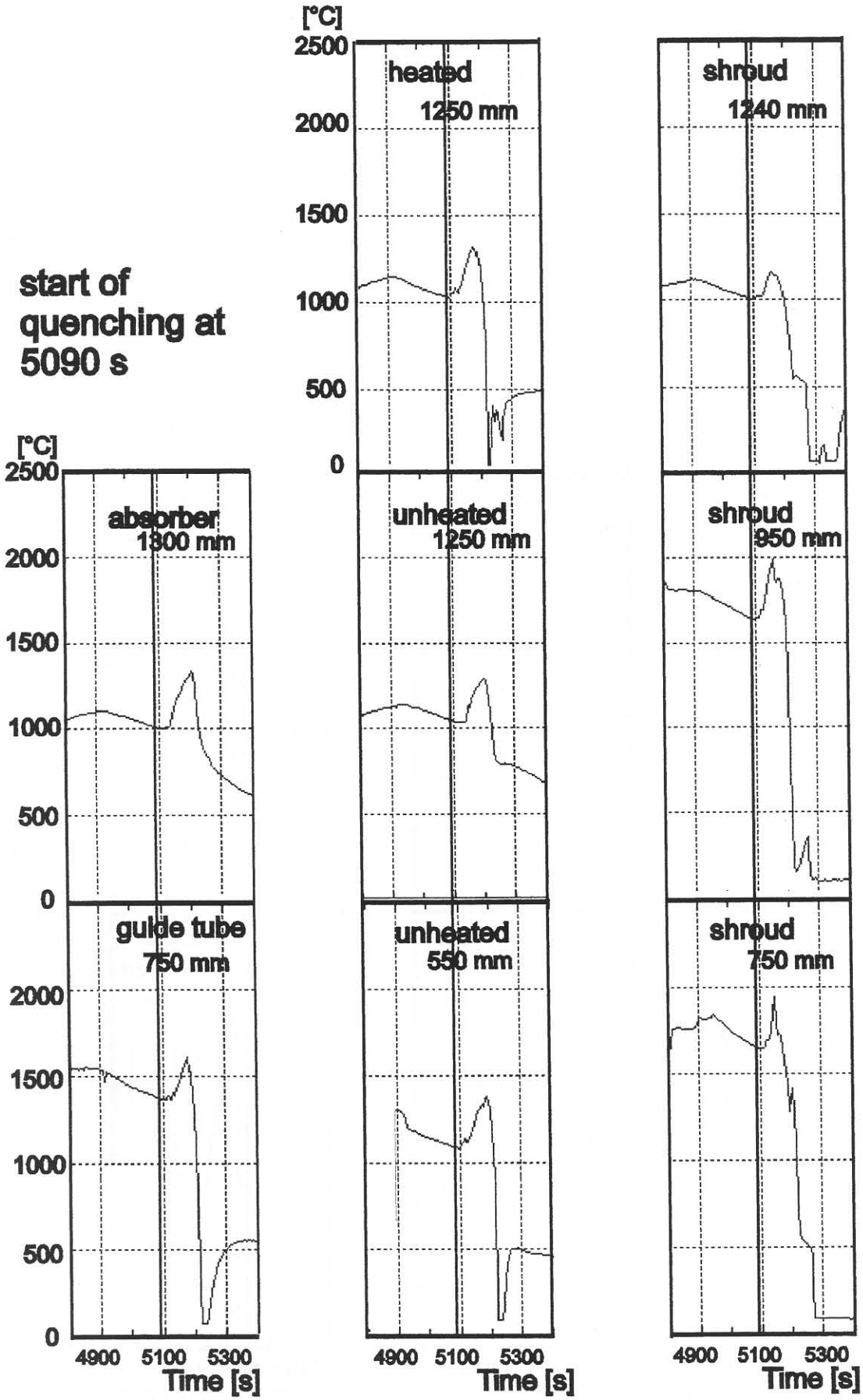

Fig.20: Temperature peaks due to quenching of test CORA-12 (PWR).

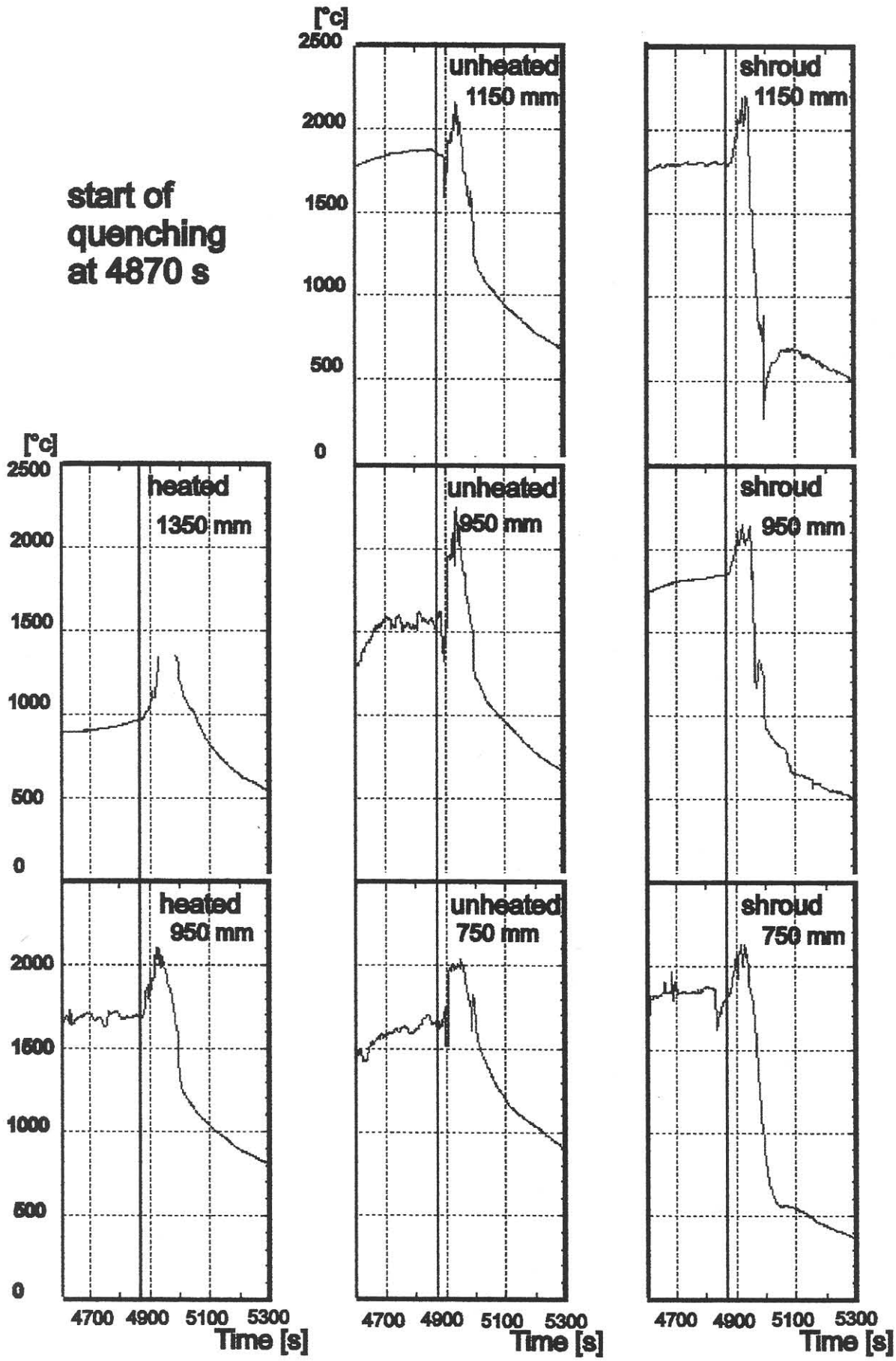

Fig.21: Temperature peaks due to quenching of test CORA-13 (PWR).

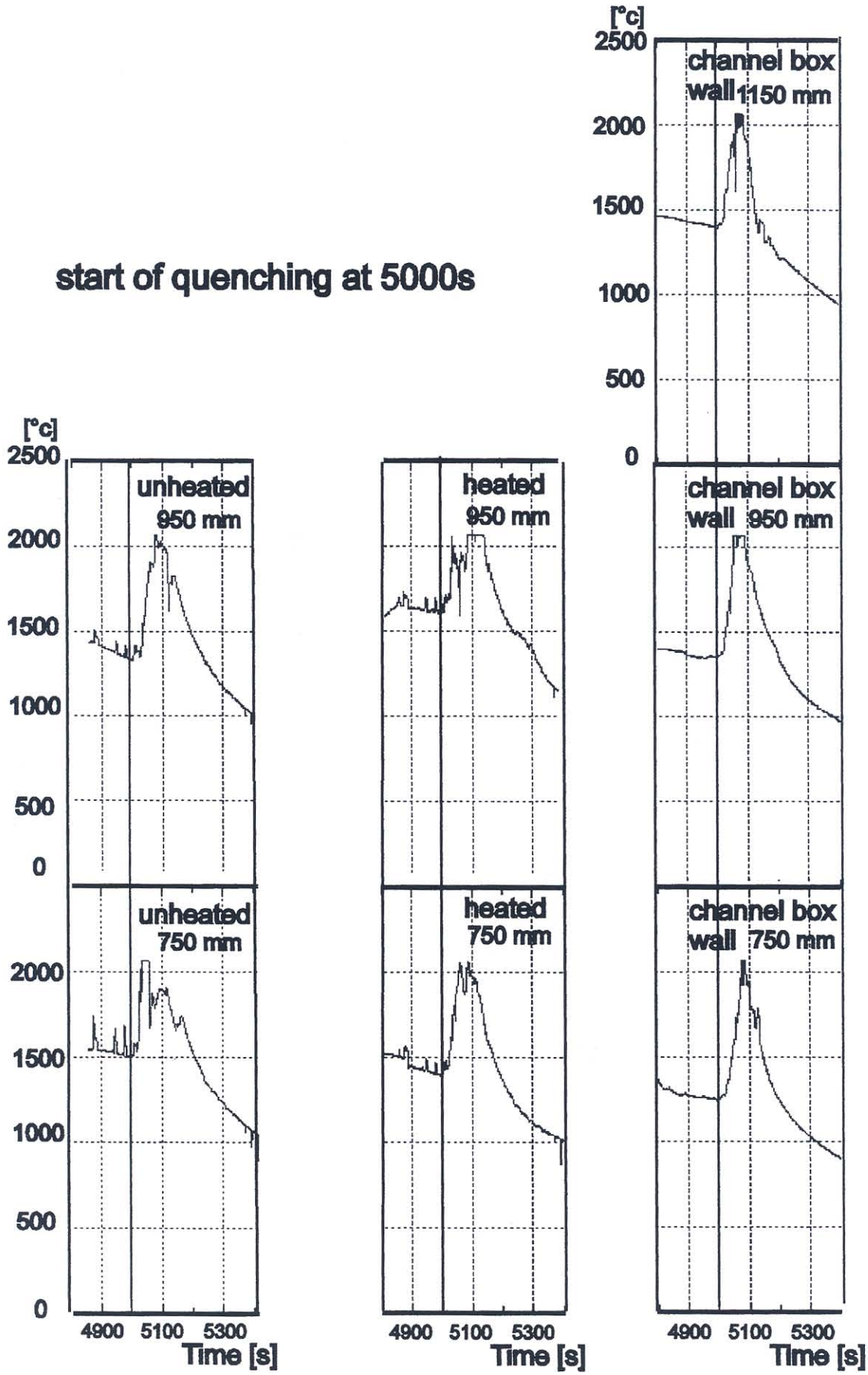

Fig.22: Temperature peaks due to quenching of test CORA-17 (BWR).

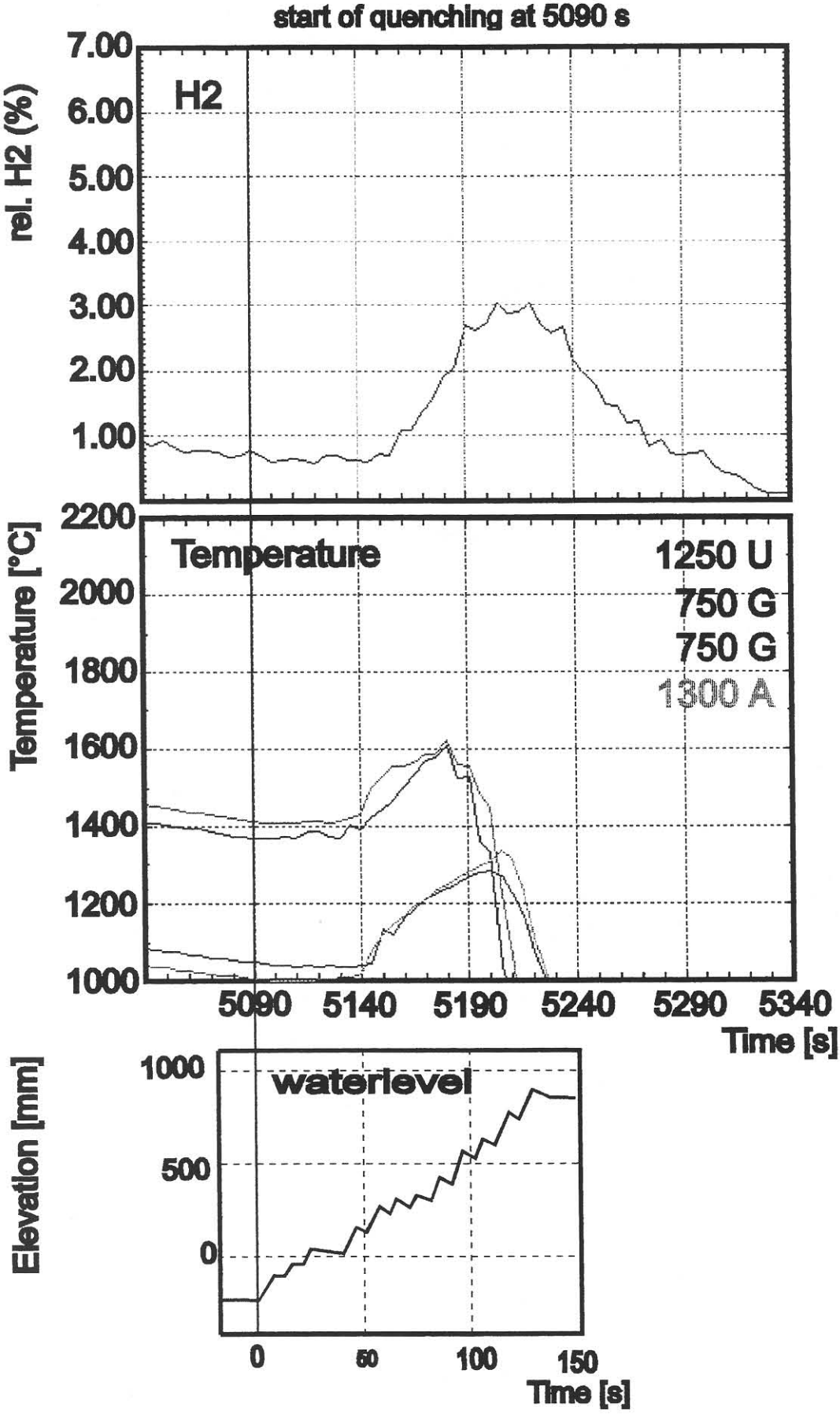

Fig.23: Comparison of hydrogen production, temperature rise and water level for test CORA-12 (PWR).

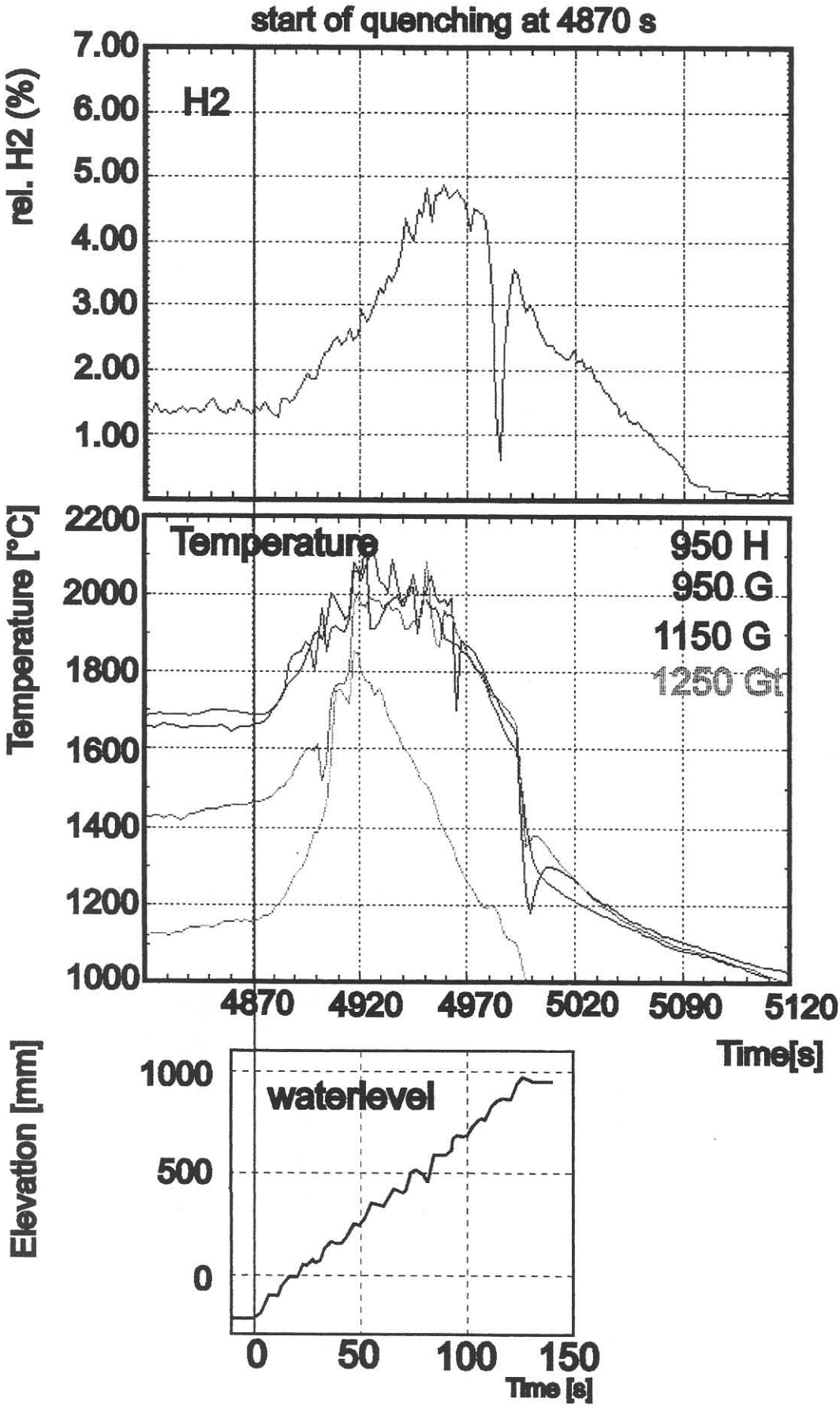

Fig.24: Comparison of hydrogen production, temperature rise and water level for test CORA-13 (PWR).

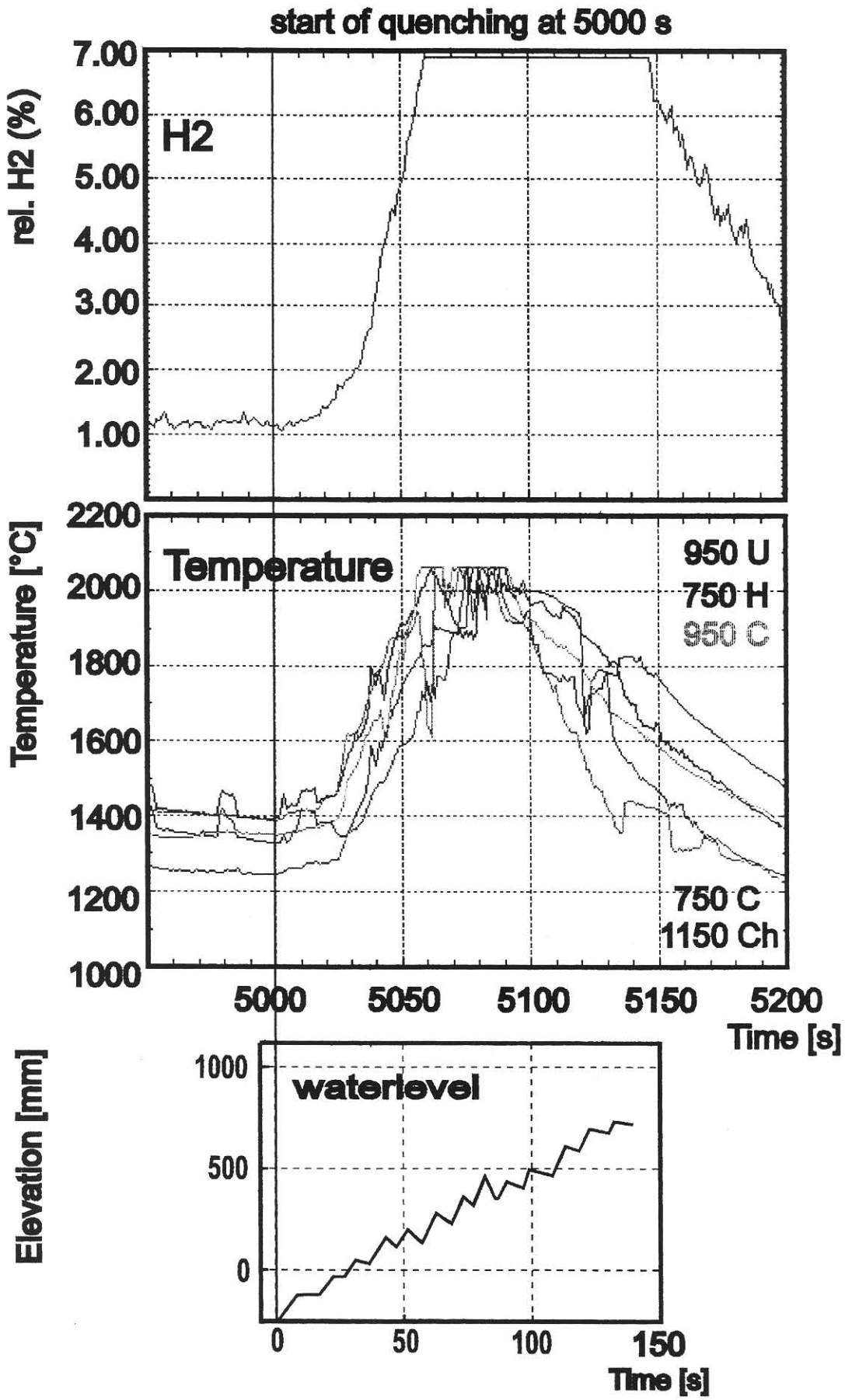

Fig.25: Comparison of hydrogen production, temperature rise and water level for test CORA-17 (BWR).

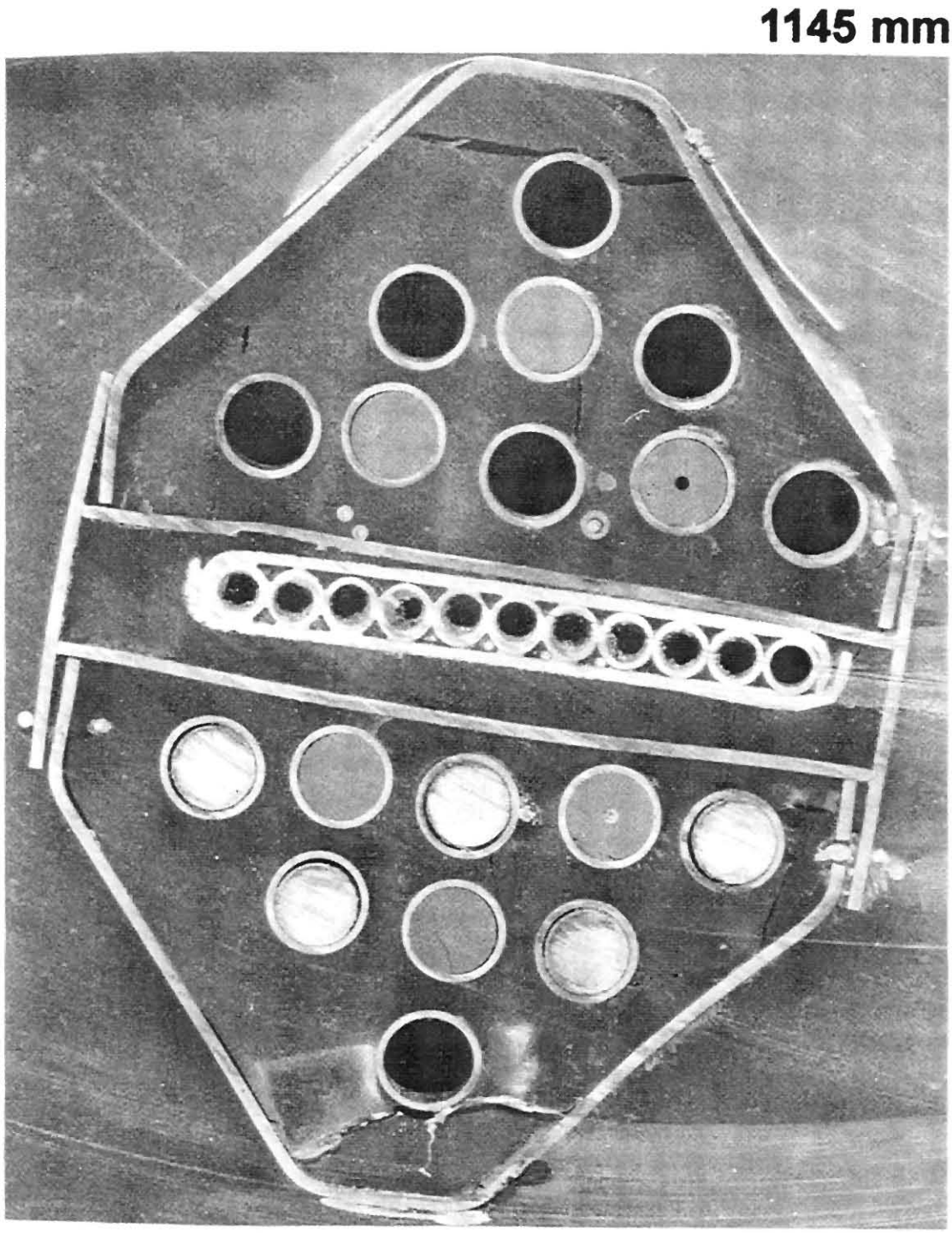

Fig. 26: Cross section of CORA-16, showing the intact structure of the BWR bundle

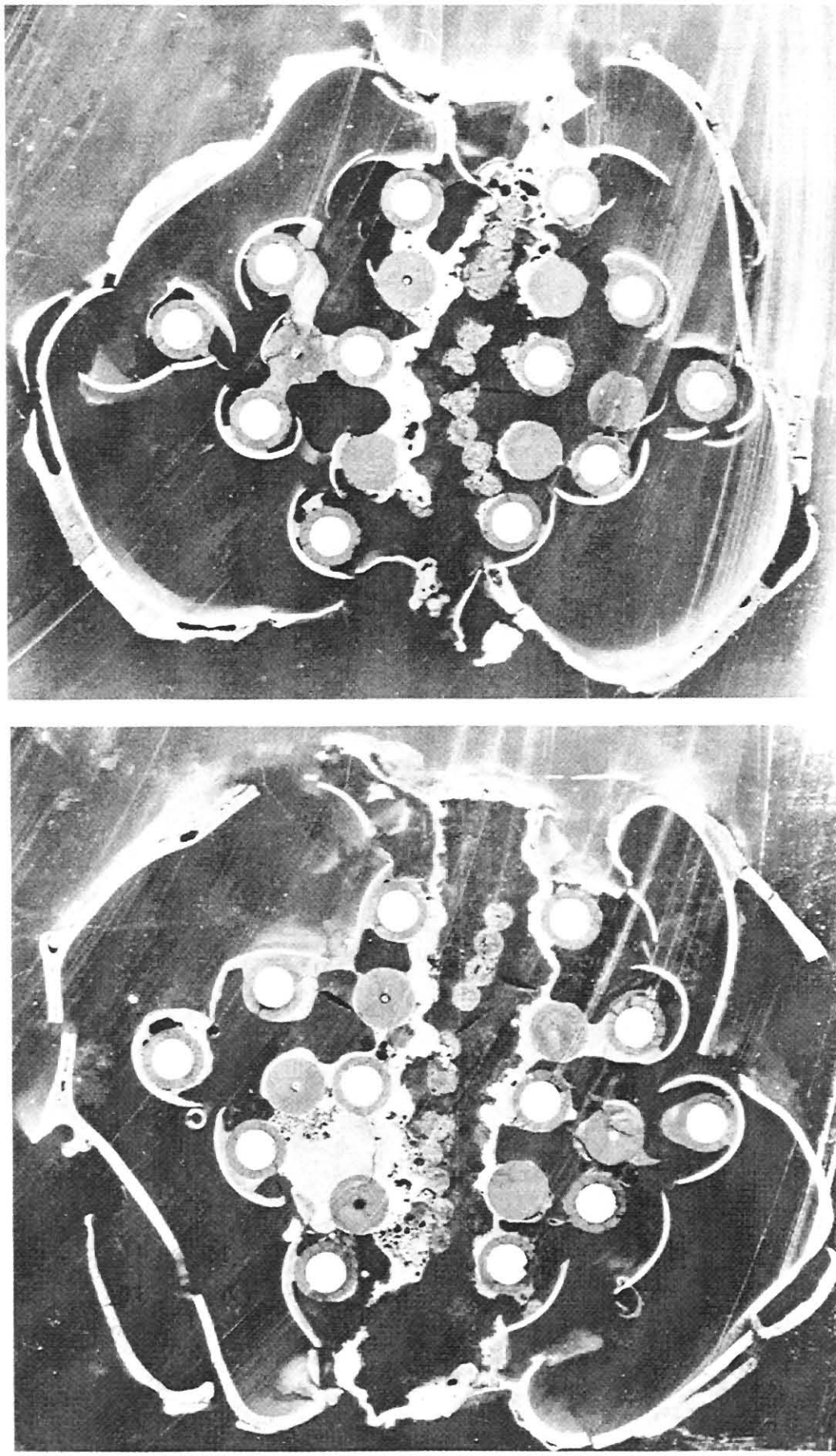

Fig. 27: Cross section of CORA-16, showing the remnant B_4C columns in the lower half of the bundle

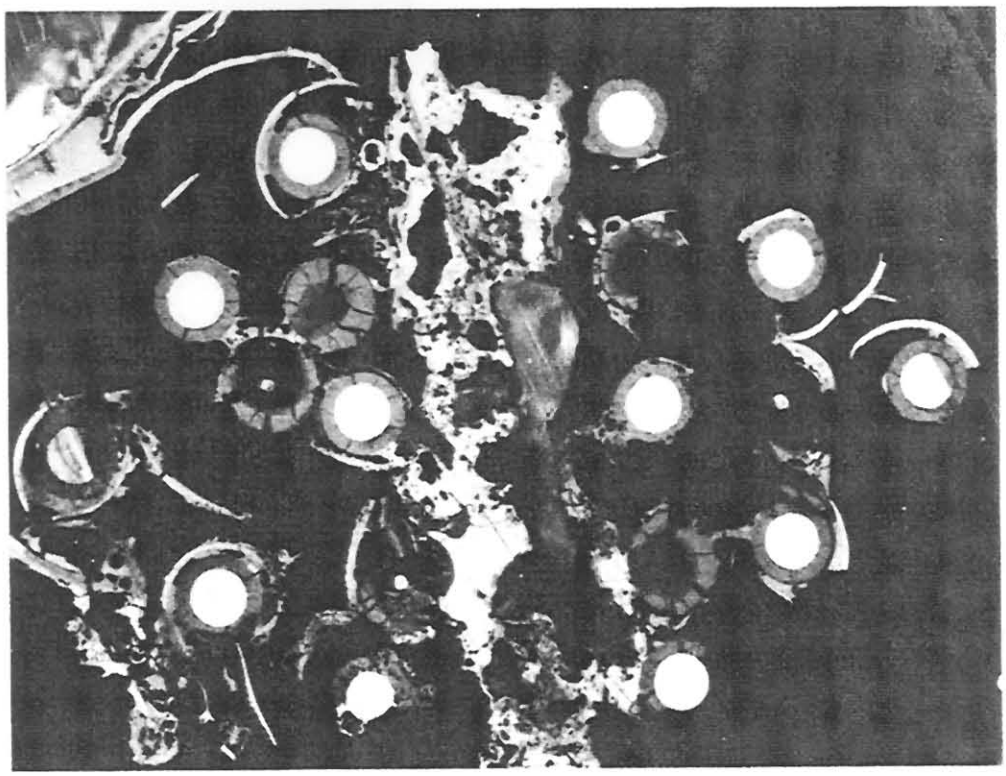

374 mm

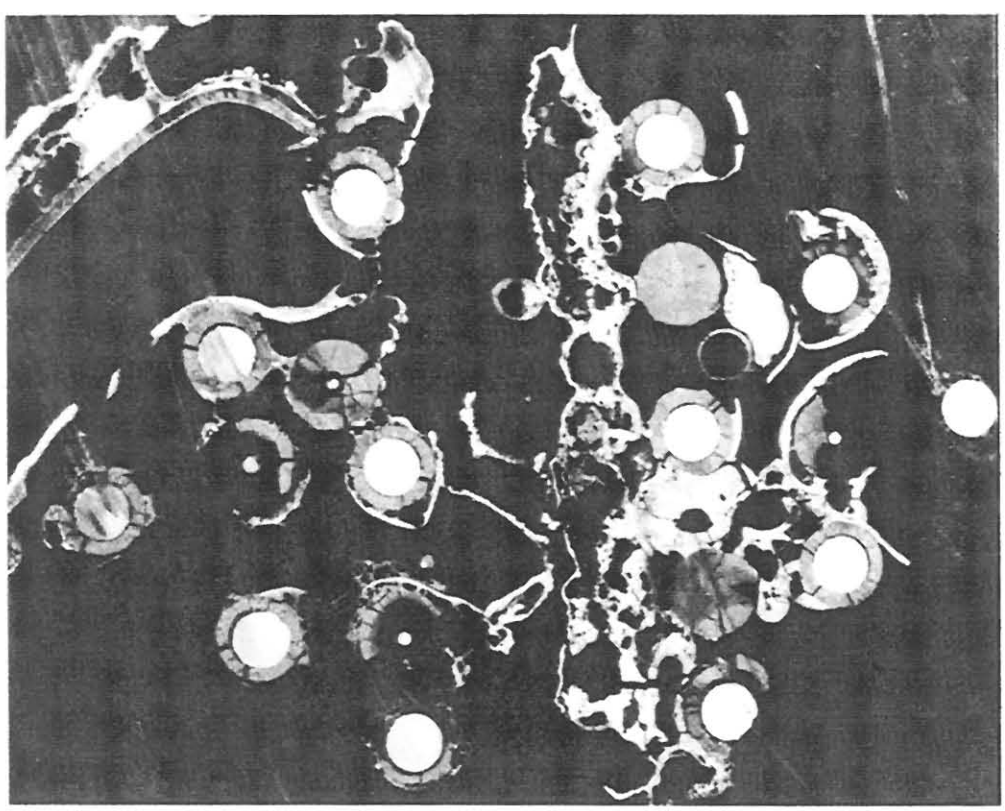

217 mm

Fig. 28: CORA-17; strong interaction of the remnant B_4C columns during the quench process